Remote Sensing Applications: Society and Environment 43 (2026) 102165

Contents lists available at ScienceDirect

Remote Sensing Applications: Society and Environment

journal homepage: www.elsevier.com/locate/rsase

Integrating remote sensing and data-driven machine learning for monitoring *Ailanthus altissima* in heterogeneous Mediterranean landscapes: a case study from Sicily

Francesco Alongi [a,d,*], Dario De Caro [a], Emilio Badalamenti [b,d], Fulvio Capodici [a,d], Rafael Da Silveira Bueno [c,d], Tommaso La Mantia [b,d], Giuseppe Ciraolo [a,d], Leonardo V. Noto [a,d]

[a] *Department of Engineering, University of Palermo, Palermo, Italy*
[b] *Department of Agricultural, Food, and Forest Sciences, University of Palermo, Palermo, Italy*
[c] *Department of Earth and Sea Sciences, University of Palermo, Palermo, Italy*
[d] *NBFC, National Biodiversity Future Center, Palermo, Italy*

A R T I C L E I N F O

Keywords:
Invasive tree species
Tree of heaven
Supervised classification
Satellite imagery
Support vector machine
Invasive management
Forest habitats

A B S T R A C T

Invasive alien plants threaten Mediterranean ecosystems, where early detection is essential for effective management and biodiversity conservation. *Ailanthus altissima* is a fast growing, highly competitive tree invader whose ecological plasticity and allelopathic properties intensify impacts on native vegetation, highlighting the need for reliable monitoring. This study develops and evaluates a remote-sensing workflow based on multitemporal PlanetScope imagery and Support Vector Machine (SVM) classification algorithm to map *Ailanthus* in ecologically sensitive areas. A training dataset was built in the heterogeneous urban park of "*La Favorita*", characterized by extensive *Ailanthus* nuclei and diverse land cover types. The trained model was then applied to the "*Vallone Piano della Corte*" Nature Reserve in central Sicily, a sensitive area currently experiencing *Ailanthus* invasion. Six SVM kernel configurations were tested and validated using field surveys and UAV-based observations. Among them, Coarse Gaussian SVM provided the most balanced performance, effectively detecting the minority invasive class while reliably discriminating dominant land cover categories. Detection accuracy depended on life stage, canopy density, and spatial configuration of *Ailanthus*, with juvenile or sparse individuals remaining difficult to detect due to spectral mixing and radiometric smoothing due to cubic convolution resampling of PlanetScope images. The use of multitemporal imagery proved essential for leveraging phenological differences between *Ailanthus* and co-occurring vegetation. The final distribution map supports monitoring, control planning, and ecological restoration, and can be integrated into ecohydrological or vegetation-dynamics models to assess invasion under changing environmental conditions. Overall, the study provides an operational and transferable workflow for invasive species monitoring in Mediterranean landscapes.

* Corresponding author. Department of Engineering, University of Palermo, Palermo, Italy.
E-mail addresses: francesco.alongi01@unipa.it (F. Alongi), dario.decaro01@unipa.it (D. De Caro), emilio.badalamenti@unipa.it (E. Badalamenti), fulvio.capodici@unipa.it (F. Capodici), rafael.dasilveirabueno@unipa.it (R.D. Silveira Bueno), tommaso.lamantia@unipa.it (T. La Mantia), giuseppe.ciraolo@unipa.it (G. Ciraolo), leonardo.noto@unipa.it (L.V. Noto).

https://doi.org/10.1016/j.rsase.2026.102165
Received 4 February 2026; Received in revised form 4 July 2026; Accepted 12 July 2026
Available online 14 July 2026

1. Introduction

Biodiversity underpins ecosystem functioning, stability, and the provision of essential ecosystem services (Harvey et al., 2017; Landi et al., 2018; Segar et al., 2020), with plant communities playing a central role as primary producers (Garnier and Navas, 2012; Raven and Wackernagel, 2020; Hoffmann, 2022). However, plant biodiversity is increasingly threatened by multiple human-driven pressures, including habitat fragmentation, climate change, pollution, and hydrological alterations (Costa et al., 2023; Noto et al., 2023; Rashid et al., 2023; Trunschke et al., 2024; Muhammad et al., 2025). Among these, invasive alien species represent a major driver of ecosystem change, as they can rapidly establish and spread in new environments, often outcompeting native species due to traits such as fast growth, high reproductive rates, broad environmental tolerance, and allelopathic effects (Lehan et al., 2013; Caracciolo et al., 2014, 2016, 2017; Gioria et al., 2023; Zhang et al., 2025).

Managing invasive plant species requires integrated strategies combining prevention, early detection, and long-term control (Clements, 2022; Colberg et al., 2024). Established populations are controlled via mechanical, chemical, or biological methods, while ecological restoration, introducing native species, improving soils, and stabilizing nutrient and hydrological cycles, enhances ecosystem resilience and reduces reinvasion risk (Culliney, 2005; Clewley et al., 2012; Badalamenti et al., 2015b; Graham et al., 2024; Raupp et al., 2024).

One particularly challenging case among invasive plant species is *Ailanthus altissima* (Mill.) Swingle, commonly known as the tree of heaven. It is a fast-growing deciduous tree of the Simaroubaceae family, native to central and eastern China and Taiwan, which was first introduced to Europe and North America in the mid-18th century for ornamental purposes and later widely used in erosion control, urban landscaping, and land rehabilitation due to its rapid growth and broad environmental tolerance (Kowarik and Säumel, 2007). These same traits have underpinned its emergence as one of the most problematic invasive alien species worldwide. Today, *Ailanthus altissima* is widely distributed across Mediterranean, temperate and subtropical regions on all continents except Antarctica (Casella and Vurro, 2013; Badalamenti et al., 2020; Terzi et al., 2021). The species is currently listed among the most harmful invasive plants by the European and Mediterranean Plant Protection Organization (EPPO) and is included in the list of Invasive Alien Species of Union Concern under EU Regulation 1143/2014, owing to its documented impacts on biodiversity and ecosystem services at the European scale. Its global expansion has been facilitated by both intentional plantings and unintentional introductions. In Europe, *Ailanthus* spread extensively during the 19th and 20th centuries along transport corridors, industrial areas, and urban centers, before progressively colonizing semi-natural and natural habitats. It is now firmly established also in South America, Australia, Africa, and the Middle East (Kowarik and Säumel, 2007; Motard et al., 2015; Walker et al., 2017; Trotta et al., 2020; Arrington, 2021; Celesti-Grapow and Ricotta, 2021; Campagnaro et al., 2022; Pisuttu, 2024; Giubilei et al., 2025; Talmot et al., 2025).

The invasiveness of *Ailanthus altissima* is driven by a combination of biological and ecological traits: fast growth rates, prolific seed production, vegetative propagation via root suckers, tolerance to abiotic stresses, and strong allelopathic effects (Ding et al., 2006; Casella and Vurro, 2013; Sladonja et al., 2015; Soler and Izquierdo, 2024). These features allow the formation of dense, often monospecific stands that suppress native vegetation and are notoriously difficult to eradicate. Reproductive versatility plays a key role in this process: the species is dioecious and produces vast quantities of winged samaras that are efficiently dispersed by wind, and in riparian environments, by water currents (Landenberger et al., 2009; Planchuelo et al., 2017; Rebbeck and Jolliff, 2018; Wagner et al., 2020). In addition, the species propagates vegetatively through root suckers and basal sprouts, enabling the rapid formation of dense clonal stands that suppress native vegetation and are extremely difficult to eradicate (Badalamenti et al., 2015a). Human-mediated dispersal further enhances its spread through the movement of contaminated soil, construction materials, and machinery. The ecological success of *Ailanthus altissima* is also tightly linked to its remarkable tolerance of harsh and heterogeneous environmental conditions. A further competitive advantage derives from allelopathy. *Ailanthus altissima* produces the quassinoid compound ailanthone, present in leaves, bark, and roots, which exerts strong phytotoxic effects on seed germination and seedling development of numerous co-occurring species (Demasi et al., 2019; Naora et al., 1982).

The situation is especially concerning in Mediterranean ecosystems, where *Ailanthus altissima* thrives in open woodlands, scrublands, and riparian areas, with the potential to jeopardize native species (Motti et al., 2021). Within this broader Mediterranean context, Sicily represents a particularly illustrative case of the species' invasive behavior. Owing to its heterogeneous landscapes, long history of land-use disturbance, and pronounced climatic gradients, the island offers a wide range of suitable habitats for invasion. Accordingly, *Ailanthus altissima* has successfully colonized diverse environments, including riverbanks, dry woodlands, abandoned agricultural areas, ruderal habitats, and degraded natural ecosystems (Badalamenti et al., 2012; Guarino et al., 2021; Minissale et al., 2023; Aleo and Bazan, 2025). Of particular concern is the ongoing encroachment of the species into protected areas, such as regional reserves and national parks, where it forms dense monospecific stands that reduce biodiversity and compromise conservation and restoration efforts (Minissale et al., 2023). The Sicilian case therefore exemplifies the ability of *Ailanthus altissima* to colonize both disturbed and ecologically sensitive habitats under Mediterranean conditions, highlighting the scale of the challenge it poses for regional biodiversity conservation.

Effective management of *Ailanthus altissima* requires robust monitoring and early detection, as interventions are more efficient and cost-effective at initial infestation stages (Constán-Nava et al., 2010; Badalamenti and La Mantia, 2013; Sladonja and Poljuha, 2018; Soler and Izquierdo, 2024; Miles et al., 2025). While accurate, traditional field surveys are labor-intensive, time-consuming, and limited in spatial coverage (Landenberger et al., 2009). Remote sensing, including satellite imagery and aerial photography, offers large-scale mapping capabilities, and its integration with machine learning algorithms enhances alien species detection by analyzing complex spectral, spatial, and temporal patterns (Tarantino et al., 2019; Qian et al., 2020; Rebelo et al., 2021; Baker et al., 2023; Naharki et al., 2023; Gao et al., 2025).

Remote sensing technologies have proven particularly effective for vegetation detection due to their ability to capture species-specific spectral and phenological characteristics across large spatial extents. Multispectral images allow the identification of subtle differences in leaf reflectance, especially in the near-infrared and red-edge bands, which are strongly related to plant physiology, chlorophyll content, and stress conditions. Moreover, the high temporal resolution of remote sensing data enables frequent observations of vegetation, which can be used to track phenological dynamics over time. Time-series analysis further enhances detection capabilities by exploiting these temporal patterns, allowing the differentiation of invasive species based on their growth cycles and seasonal behavior. On the other hand, Unmanned Aerial Vehicles (UAVs) provide very high-resolution data and enable detailed monitoring of sensitive or heterogeneous areas, thus complementing satellite-based remote sensing approaches (Qian et al., 2020; Naharki et al., 2023). However, UAV-based surveys are generally less flexible and scalable than satellite acquisitions, due to logistical constraints, longer data collection times, and the need for extensive processing workflows. Despite these limitations, UAV data are extremely valuable for model calibration and validation, as their finer spatial resolution allows for more accurate *in situ* truthing of classifications derived from satellite imagery.

Thus, satellite images serve as key input features for machine learning models, including spectral bands, vegetation indices, textural metrics, and temporal signatures extracted from time-series analysis. The integration of machine learning algorithms significantly improves classification accuracy by handling high-dimensional and complex datasets. Supervised approaches such as Random Forest and Support Vector Machines can automatically learn discriminative features from spectral, spatial, and textural information. These models are particularly effective in heterogeneous landscapes, where traditional classification methods often struggle (Basheer et al., 2024; Gyamfi-Ampadu et al., 2020; Song and Zhang, 2025; ZandKarimi et al., 2025).

This study presents a remote sensing-based, data-driven classification model specifically developed to detect *Ailanthus altissima* and potentially monitor its dynamics. To date, the application of machine learning approaches, such as SVM, combined with satellite images for the specific detection of *Ailanthus altissima* remains limited, highlighting a relevant research gap. Existing studies have primarily focused on the detection of invasive species using remote sensing and machine learning techniques across different species and geographic contexts, providing a methodological foundation that this work builds upon (Rebelo et al., 2021). The model was designed to operate with high-resolution satellite imagery; in particular, data from the PlanetScope constellation were used, offering eight spectral bands, a spatial resolution of 3 m, and a daily revisit frequency. Thus, the integration of multitemporal PlanetScope images constitutes a major methodological advantage of this study, as it leverages a recent Earth observation dataset characterized by high spatial and temporal resolution, allowing a detailed representation of seasonal vegetation dynamics and providing a consistent observational basis for the analysis across different phenological stages; however, the approach remains constrained by the 3 m spatial resolution, which limits the detection of small, sparse, or juvenile *Ailanthus altissima* individuals and increases mixed-pixel effects at class boundaries. This multitemporal representation is particularly important for *Ailanthus altissima* detection, as it enables the model to exploit phenological differences between the target species and surrounding vegetation that may be difficult to distinguish using single-date imagery. Satellite-derived variables were used as input features for the classification process. The core of the model is based on the Support Vector Machine (SVM) algorithm (Cortes and Vapnik, 1995; Burges, 1998), with multiple SVM configurations assessed to evaluate the ability to discriminate *Ailanthus altissima* from other land cover types. The evaluation of configurations and the optimal choice were conducted using several class-specific indicators and global accuracy measures. The systematic evaluation of multiple SVM kernels under identical training conditions was designed as a controlled benchmarking experiment, ensuring a fair and consistent comparison of model configurations and enabling a robust assessment of their relative performance under equivalent experimental settings. The approach was implemented across two distinct study areas: one used for model training and calibration, and another independent area used for model validation, to assess its transferability and robustness. This cross-site training and validation design represents a key strength of the study, as it enables a fully independent assessment of model performance in a spatially distinct context, providing a more realistic evaluation, compared to conventional approaches, based on random data partitioning within a single area. More specifically, the tAOI-to-AOI framework was intentionally designed as a transferability experiment, allowing the assessment of model generalization capabilities under different environmental and ecological conditions rather than as a simple within-site validation exercise. Furthermore, the validation phase was supported by an *in situ* survey conducted using UAV, which provided very high spatial resolution data. This data served as reliable ground reference information, enhancing the accuracy assessment of the satellite-based classification results. Thus, the integration of UAV-derived ground truth with satellite-based classification provides a multi-scale validation framework, strengthening the consistency and reliability of the classification results across spatial scales. In this context, the primary objective of the study is to develop and evaluate a multi-scale, remote sensing-based workflow for the detection and monitoring of *Ailanthus altissima* using multitemporal PlanetScope imagery, UAV-derived reference data, and supervised machine-learning classification. Within this framework, a secondary analytical objective is to systematically compare different SVM kernel configurations under identical training conditions to identify the most suitable model for detecting a spatially rare invasive species under strong class-imbalance conditions. Model performance and selection were evaluated using both class-specific and global metrics, with particular emphasis on F1-score, Balanced Accuracy, and statistical significance analyses. The study also aims to assess the potential and the limitations of an approach that relies exclusively on satellite-derived information and does not require any a priori knowledge of the phenological or structural characteristics (e.g., canopy architecture, growth stage) of the invasive species. These conditions include class imbalance between the target species and other land cover types, as well as sensor-related constraints intrinsic to high-resolution satellite images.

2. Materials and methods

2.1. Study sites

Two study sites were considered, each with a complementary role.

2.1.1. Urban park of "La Favorita"

The training area of interest (hereinafter referred to as tAOI) is located within "*La Favorita*" Oriented Nature Reserve, in the urban context of Palermo (38°09′56.0″N 13°20′20.1″E; Fig. 1). The tAOI covers approximately 10 km^2 (∼1000 ha) and it was selected as the training site due to its extensive and well-documented presence of *Ailanthus altissima* and its heterogeneous land cover mosaic. In this area, large monospecific stands of *Ailanthus,* particularly concentrated at the foot of Monte Pellegrino, coexist with urban infrastructures (e.g., roads, buildings), agricultural orchards, bare soil patches, a variety of native vegetation, and water bodies (i.e., the Tyrrhenian Sea along the eastern boundary), providing an ideal setting for generating representative training samples across all target classes. Despite its proximity to densely populated areas, anthropogenic disturbance within the reserve is minimal due to strict conservation regulations prohibiting new construction. Existing infrastructure is limited to a few connecting roads, which are maintained but not expanded. These characteristics make "*La Favorita*" an ideal site for generating representative training samples across all target classes and for modeling the spectral behavior of *Ailanthus* altissima in a complex environment.

2.1.2. "Vallone Piano della Corte" Nature Reserve"

While the tAOI provides a controlled and well-characterized environment for model training, the area of interest (hereinafter referred to as AOI) represents an ecologically sensitive protected natural area, characterized by a rich native flora and currently affected by the expansion of several *Ailanthus* nuclei posing a serious threat to local biodiversity and ecosystem stability and functioning, where the model is applied and validated. The AOI is located within the "*Vallone Piano della Corte*" Nature Reserve (37°39′09.0″N 14°28′51.6″E), in central-southern Sicily, in the innermost mountainous sector of the Simeto River basin, the largest river in Sicily in terms of catchment area. The reserve lies in a predominantly hilly and mountainous landscape characterized by a mosaic of natural vegetation, agricultural plots, and semi-natural open spaces. The AOI, considered in this study, covers approximately 20 ha along the central reach of the main tributary of the reserve. Its geomorphology is defined by two contrasting hillsides: a north-facing slope densely vegetated and dominated by *Quercus pubescens* Willd., and a south-facing slope with sparse vegetation, exposed soils, and rocky outcrops in the upper sections. On this latter slope, a major infestation of *Ailanthus altissima* has established. The largest and most consolidated nucleus forms a discontinuous patch adjacent to the streambed, accompanied by three smaller clusters, one of which consists mainly of young individuals, indicating active colonization and vegetative expansion. Overall, the invaded area covers ∼2700 m^2, corresponding to ∼1.5% of the AOI (Fig. 2).

Despite differences in class representation, the reserve exhibits a land cover composition comparable to that of the training site,

Fig. 1. Illustrative figure of the tAOI. The dashed red rectangle highlights the tAOI including "*La Favorita*" park at the base of Monte Pellegrino. The background image is a natural color optical image obtained from Google Earth. The inset map (upper right) shows the location of the tAOI within Sicily.

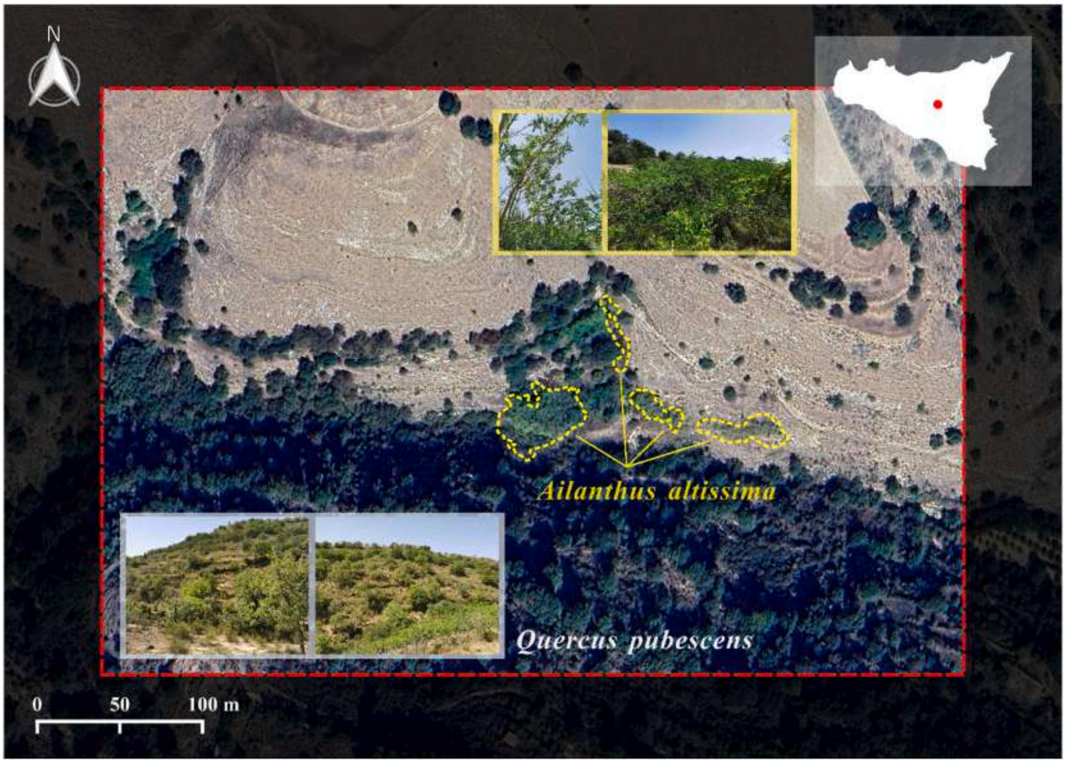

Fig. 2. Illustrative figure of the AOI (red dashed rectangle) within the "*Vallone Piano della Corte*" Nature Reserve. The background image is a natural color optical image obtained from Google Earth. Clusters of *Ailanthus altissima*, mapped based on field surveys, are shown with yellow dashed polygons. Representative field pictures of *Ailanthus altissima* and *Quercus pubescens* are also included. The inset map (upper right) indicates the location of the AOI within Sicily region.

allowing a consistent application of the trained model configurations.

Climatically, the AOI is representative of inland Mediterranean environments, with a marked seasonal regime. Mean annual precipitation ranges between 500 and 650 mm, concentrated between October and March (Arnone et al., 2013; Treppiedi et al., 2026). Summers (June – August) are typically hot and dry, with mean monthly temperatures reaching 28-30°C in July and August and daily maxima frequently exceeding 35°C. Winters are mild, with average temperatures of 5 – 7°C in January and February, occasionally dropping below freezing during nighttime frost events (Viola et al., 2014).

Soils are predominantly sandy, with moderate permeability and limited water-holding capacity. The upper sections of the south-facing slope are shallow and rocky, favouring stress-tolerant species. Under these edaphic constraints, *Ailanthus altissima* thrives thanks to its ecological plasticity and competitive traits.

2.2. Data acquisition and pre-processing

The classification model was developed to map the spatial distribution of *Ailanthus altissima* by integrating multispectral remote sensing data with a supervised classification algorithm. Spectral and temporal information were jointly exploited to distinguish the target species from other land cover types and to capture the spatial structure of invaded areas. Within this framework, high-resolution multispectral imagery was acquired for both the tAOI and the AOI from the PlanetScope satellite constellation. PlanetScope "Ortho scene" products are distributed at a nominal spatial resolution of 3 m and benefit from an almost daily revisit frequency, allowing consistent fine-scale monitoring over time. However, a cubic-convolution resampling of the original sensed radiances is applied (Marta, 2018; Shields et al., 2025); thus, a 4x4 neighborhood (16 raw pixels) interpolation is employed in computing the final radiance (and thus, the reflectance) value of each pixel. This procedure inevitably modifies the original radiometric signal through spatial averaging and interpolation. The cubic-convolution process may introduce subtle smoothing effects and additional uncertainty in spectral responses (Anger et al., 2019), with potential implications for classification accuracy.

Each PlanetScope's SuperDove SR_8 b_harmonized image includes surface reflectance of eight spectral bands, Coastal Blue (431–452 nm), Blue (465–515 nm), Green I (513–549 nm), Green (547–583 nm), Yellow (600–620 nm), Red (650–680 nm), Red Edge (697–713 nm), and Near Infrared (NIR) (845–885 nm), enabling discrimination of vegetation types based on reflectance and phenology. The product is radiometrically calibrated, orthorectified, and provided as atmospheric-corrected surface reflectance; atmospheric correction is performed using the 6SV2.1 radiative transfer model, incorporating ancillary data from MODIS to account for atmospheric effects on the signal observed at the sensor for the PlanetScope constellation (Frazier and Hemingway, 2021). These preprocessing steps are included in the PlanetScope SR_8 b_harmonized product and were not performed by the authors. The only processing steps applied in this study consisted of image selection, visual quality screening, and the construction of the multitemporal image stacks described below.

To capture intra- and inter-annual variability, one cloud-free image per month was selected separately for the tAOI and AOI over the period 2021-2024. Cloud screening was performed through a visual inspection of the images over the study areas. Only cloud-free acquisitions were retained for analysis; therefore, no gap-filling, interpolation, or replacement procedures were required within the multitemporal dataset. Furthermore, acquisitions were consistently selected near the middle of each month, to minimize seasonal edge effects and better represent the typical intra-month surface conditions, thereby improving temporal comparability across the dataset. This selection criterion was adopted to ensure temporal consistency among years and to minimize variability associated with short-term phenological transitions occurring at the beginning or end of each month. All images were downloaded from the Planet platform (https://www.planet.com/explorer/) under a member license, resulting in a total of 48 images for each site. The only pre-processing step applied in this study consisted of the construction of multitemporal image stacks. Monthly PlanetScope images were stacked across spectral bands and years to create multitemporal data cubes for each study area. Each stack comprised 384 layers (12 months × 4 years x 8 spectral bands = 384 layers). Layers were ordered chronologically according to acquisition date, preserving the original eight spectral bands for each monthly image before appending the subsequent monthly acquisition to the stack. Stack generation was performed using QGIS (released 3.4.3) and no additional pre-processing steps were applied. This stacking step enabled the joint exploitation of spectral and temporal information, allowing the classification model to capture phenological dynamics and temporal consistency in the spatial distribution of *Ailanthus altissima*. A key assumption underlying this approach is that the spatial distribution of *Ailanthus* clusters within both tAOI and AOI remained stable over the 2021-2024 period. Examples of monthly satellite images acquired in consecutive years are shown in Fig. 3.

The use of multitemporal PlanetScope images represents a key methodological strength, as their high spatial and temporal resolution enables the characterization of seasonal vegetation dynamics and supports a temporally consistent classification framework; however, the study is inherently constrained by the 3 m spatial resolution, which limits the detection of small, sparse, or juvenile *Ailanthus altissima* individuals and increases the influence of mixed pixels along class boundaries.

2.3. SVM algorithm and training procedure

The classification model is based on the Support Vector Machine (SVM) algorithm, which defines optimal decision boundaries in feature space and is capable of handling both linear and non-linear class separability (Cortes and Vapnik, 1995; Burges, 1998). The SVM implementation available in MATLAB® (release 2025a) was adopted, testing multiple model configurations based on different

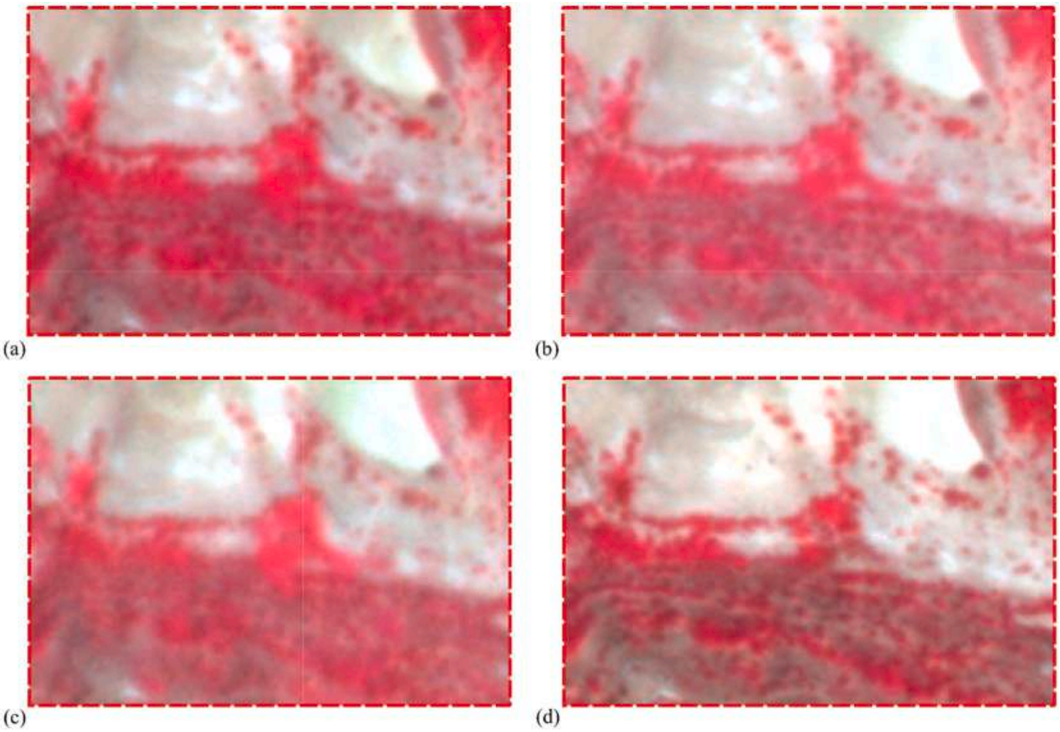

Fig. 3. Example of PlanetScope false-color composites (NIR-Red-Green) of the AOI. All images were acquired in July: (a) 02/07/2021, (b) 07/07/2022, (c) 12/07/2023, and (d) 16/07/2024.

kernel functions characterized by increasing levels of flexibility and complexity, using the Classification Learner app within the Statistics and Machine Learning Toolbox™ (release 2025a). The selection of SVM as the final classification model was performed following a comprehensive preliminary analysis aimed at assessing the reliability and performance of all classification algorithms available within the Classification Learner Toolbox. This analysis involved a systematic comparison of multiple model families under consistent training conditions, evaluating both classification performance and computational efficiency. The full description of this model selection procedure, including quantitative comparisons and validation analyses, is provided in the Supplementary Material. All models were implemented using the default hyperparameter settings provided by the Classification Learner app, ensuring methodological consistency and reproducibility. In particular, the box constraint parameter was set to its default value ($C = 1$), which controls the balance between allowing misclassification of training samples and maintaining a smooth and generalized decision boundary. In the context of this study, this parameter influences how strictly the model separates the spectral-temporal signatures of *Ailanthus altissima* from other land cover classes. Predictor standardization was enabled (i.e., all features were centered and scaled to zero mean and unit variance), ensuring that spectral bands and temporal features with different numerical ranges contribute equally to the classification process. No user-defined random seed was specified, and all models were trained using the default settings of the MATLAB Classification Learner environment. The multiclass problem was handled using the default one-vs-one strategy, in which the classification task is decomposed into all pairwise class combinations. Each pairwise classifier focuses on distinguishing between two specific land cover classes (e.g., *Ailanthus* vs other vegetation), and the final class assignment for each pixel is determined through a majority voting scheme. This approach is particularly suitable for heterogeneous landscapes, where spectral overlap between classes can vary depending on the specific class pair. In the MATLAB® framework, kernel functions determine how input features are mapped into higher-dimensional spaces, thereby controlling the shape and complexity of the resulting decision boundaries. Specifically, the following kernel functions were evaluated:

- linear kernel (Linear), which does not transform the input data and assumes that classes are separable by a linear hyperplane in the original feature space, resulting in simple and easily interpretable decision boundaries;
- polynomial kernels (Quadratic and Cubic), which introduce non-linear feature interactions and allow progressively more complex curved decision surfaces, enabling the model to capture moderate non-linear relationships among features;
- Gaussian Radial Basis Function (RBF) kernel, which measures similarity between samples as a function of their distance in feature space and implicitly projects the data into an infinite-dimensional space, allowing highly flexible and complex non-linear class separation.

The behavior of the RBF kernel is controlled by the scale parameter γ, which regulates the influence of individual training samples and, consequently, the smoothness of the decision boundary. Smaller γ values correspond to narrower Gaussian functions, yielding more localized decision regions that are sensitive to fine-scale spectral-temporal variability, whereas larger values produce broader Gaussian functions and smoother, more generalized decision boundaries that are less sensitive to noise and outliers. Based on this principle, three RBF configurations were tested: (i) Fine Gaussian ($\gamma = 0.25$), Medium Gaussian ($\gamma = 1$), and Coarse Gaussian ($\gamma = 4$), representing increasing levels of boundary smoothness and decreasing model complexity. Model training and internal validation were performed using the default cross-validation procedure implemented in the MATLAB Classification Learner environment.

The training of all SVM configurations was conducted using the multitemporal satellite data cube of the tAOI. Training polygons were manually delineated within the tAOI for each of the five land cover classes: (i) *Ailanthus altissima*, the target species, (ii) bare soil, comprising exposed mineral surfaces, rocky outcrops, and eroded slopes, characterized by high red reflectance and low temporal variability, (iii) other vegetation, grouping all vegetated areas not classified as *Ailanthus altissima*, essential for separating the invasive species from the surrounding vegetative matrix, (iv) urban elements, including roads, paved surfaces, and buildings, and (v) water bodies. Polygon delineation was based on visual interpretation of very high-resolution imagery from Google Earth combined with field surveys, allowing a reliable identification of invaded patches within the urban matrix. Each pixel within the polygons was treated as an independent training sample, represented by a feature vector including spectral values from all acquisition dates. In this way, both spectral and temporal variability were embedded in the learning process. All pixels contained within the training polygons were retained as training samples. No minimum-distance threshold, buffering procedure, or exclusion of edge pixels was applied, as the objective was to preserve the full spatial and spectral-temporal variability represented by each training class. While this pixel-based sampling strategy may introduce some degree of spatial dependence among neighboring observations, the final assessment of model performance was conducted on an independent validation area spatially separated from the training site, thereby reducing the potential influence of spatial autocorrelation on the reported performance estimates.

Mathematically, training consists in solving a convex optimization problem, meaning that the algorithm searches for a single, globally optimal decision boundary (or hyperplane in higher-dimensional space) that maximizes the margin between classes while allowing controlled misclassification of some samples. The resulting classification functions are fully defined by a subset of the training samples, the support vectors, which lie closest to the class boundaries and exert the greatest influence on the model. Using the same training polygons for all SVM configurations ensures that differences in performance reflect only the choice of kernel function. The choice of kernel affects the shape and flexibility of the learned boundaries: the linear kernel produces straight hyperplanes; polynomial kernels allow curved boundaries; and Gaussian RBF kernels enable highly non-linear, complex boundaries.

The final trained model configurations are defined by a subset of the training samples which are the support vectors, along with their associated weights, the kernel function, and its parameters. These structures determine the decision functions used to classify new pixels: for each pixel, the functions evaluate a weighted combination of its similarity to the support vectors in the transformed feature space, plus a bias term. In this way, the resulting model is compact, generalizable, and capable of classifying any pixel in the AOI based on the spectral-temporal patterns learned from the tAOI.

Training polygons were derived to capture intra-class variability and spatial heterogeneity. For *Ailanthus altissima*, polygons were specifically constrained by the precise locations of individual trees and nuclei collected during dedicated field surveys, ensuring accurate spectral-temporal representation. Multiple polygons per class were spatially distributed across the tAOI (Fig. 4) to account for differences in illumination, background conditions, and phenological stages, while reducing the risk of model overfitting (Shebl et al., 2022). The resulting training dataset includes all identified *Ailanthus* altissima individuals and nuclei within the tAOI (2393 pixels), together with polygons representing urban elements such as roads, buildings, and other impervious surfaces (9534 pixels), bare soil areas devoid of vegetation throughout the year (9815 pixels), water bodies corresponding to marine surfaces within the tAOI (14647 pixels), and other vegetation, encompassing all non-*Ailanthus* arboreal and shrub covers (52423 pixels).

2.4. Land cover reference mapping in the AOI

To reconstruct the spatio-temporal dynamics of *Ailanthus altissima* within the AOI and generate a reference dataset to validate classification outputs, a diachronic analysis was performed using historical cartography, satellite imagery, and UAVs surveys. The objectives were: (i) to estimate the timing of initial establishment, and (ii) to produce a spatially explicit land cover map representing the current cover status. A detailed description of the diachronic analysis aimed at reconstructing the timing of the invasion is provided in the Supplementary Material. For the second objective, instead, two UAV photogrammetric surveys conducted in 2024 added a detailed reference layer for mapping the current distribution of *Ailanthus altissima* within the AOI. The reference mapping was based on an integrated approach combining visual interpretation, UAV-based remote sensing, and direct field observations. UAV surveys were conducted over the AOI on June 11th and July 30th, 2024, covering ~10 ha and encompassing all known nuclei of the species. Flights were carried out using an ExaCopter EVO platform equipped with a high resolution RGB camera, acquiring imagery at a ground sampling distance of 0.02 m/px. To achieve this spatial resolution, the UAV flew at an altitude of approximately 60 m above ground level with an average flight speed of 1 m/s. Image acquisition was planned to ensure 70% frontal and lateral overlap between consecutive acquisitions, enabling the generation of high-quality orthomosaics. The ExaCopter EVO is a professional hexacopter designed for surveillance and mission-critical operations, featuring stable GPS-assisted flight, modular payload support, and real-time video transmission, equipped with an RGB 4 K camera capable of recording smooth 60FPS footage for high-quality aerial imaging and detailed situational awareness. The acquired UAV RGB images were pre-processed using PIX4D software (https://www.pix4d.com/), to generate georeferenced orthomosaics. These products allowed detailed visual interpretation and precise delineation of *Ailanthus altissima* clusters, including their spatial extent and internal structure. Both the validation map and the land cover reference labels (Fig. 5) were generated from UAV imagery, systematically supported by field surveys, during which species presence was confirmed *in situ* and the boundaries of invaded patches were verified using GPS positioning. All land cover units within the AOI were manually digitized and assigned to classes based on direct field evidence and visual interpretation of the high-resolution UAV orthomosaics,

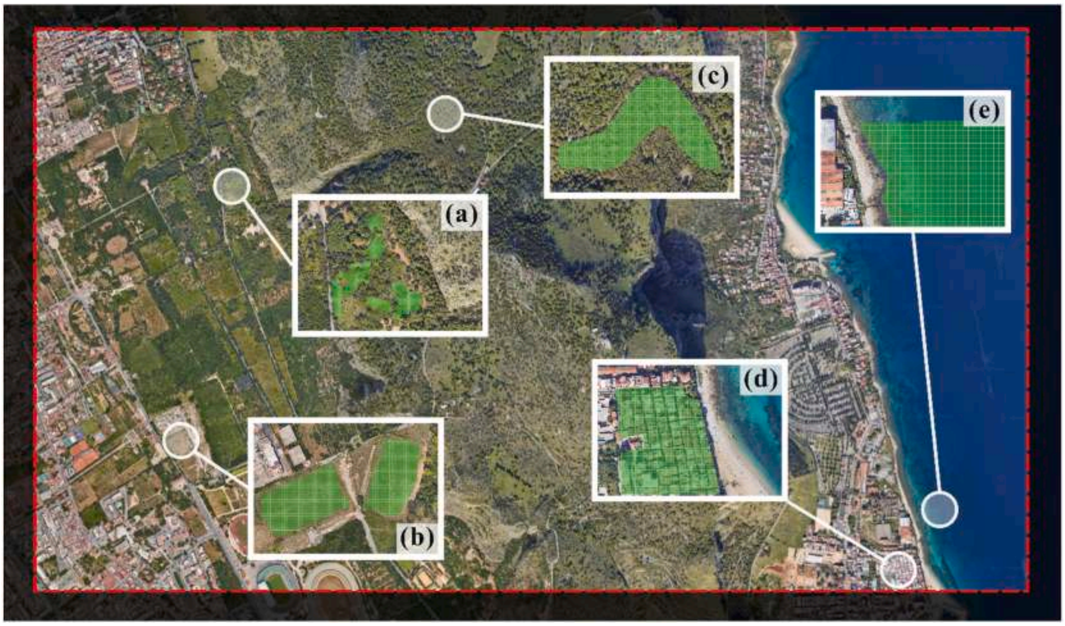

Fig. 4. Examples of training polygons within the tAOI. Inset boxes illustrate representative polygons for the considered land cover classes (i.e., *Ailanthus* (a), bare soil (b), other vegetation (c), urban elements (d), and water bodies (e)). Other vegetation includes all non-*Ailanthus altissima* vegetated covers, including other trees and shrubs. Only a subset is displayed; additional polygons were delineated to ensure comprehensive class representation and spatial heterogeneity.

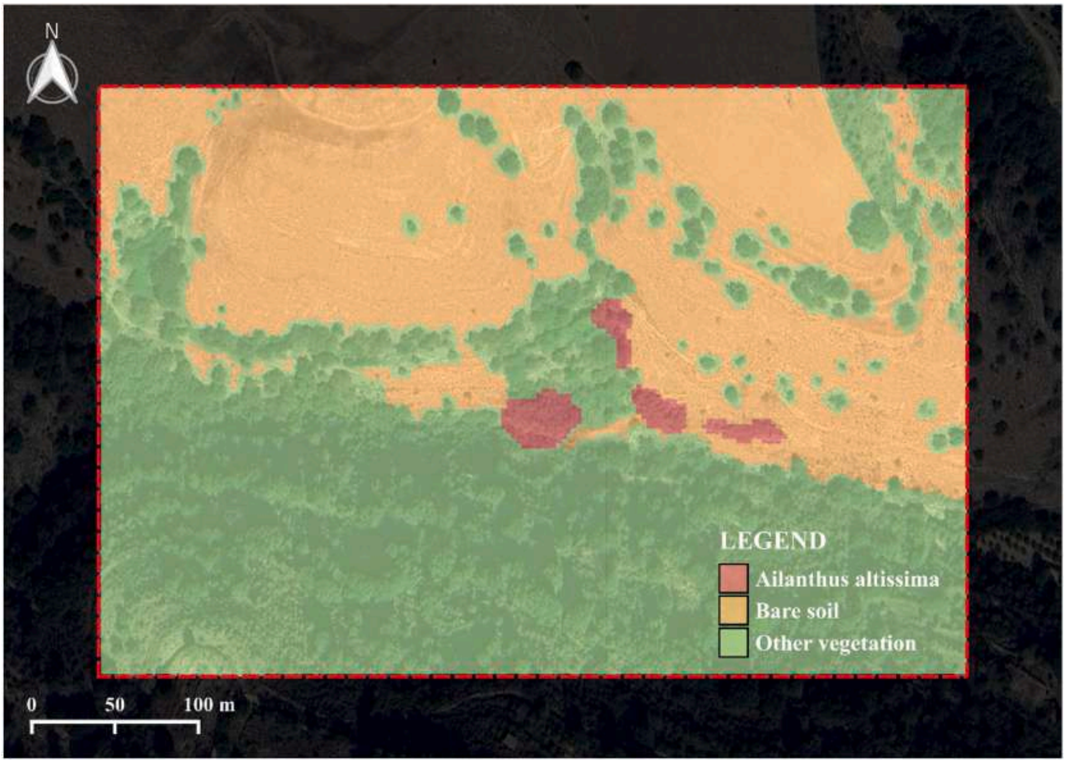

Fig. 5. Land cover reference map of the AOI derived from high-resolution UAV imagery and field-based GPS measurements. The background image is a natural color optical image obtained from Google Earth.

using the same class definitions adopted for model training (i.e., *Ailanthus altissima*, bare soil, and other vegetation). The resulting validation dataset comprises 331 pixels belonging to *Ailanthus altissima*, 7604 pixels classified as bare soil, and 12306 pixels corresponding to other vegetation. The relatively limited number of *Ailanthus* pixels reflects the actual spatial distribution of the species within the AOI, where it occurs in localized patches and nuclei embedded within a broader matrix of natural land cover types. For consistency with the multispectral PlanetScope imagery used for classification purposes, the digitized map was converted to a raster map with the PlanetScope grid (i.e., 3 m spatial resolution), allowing direct comparison and accuracy assessment at the same resolution. The conversion was performed by overlaying the PlanetScope grid onto the digitized map and assigning each pixel to the class corresponding to the dominant area. Cases of equal class representation within a pixel did not occur in the validation dataset; therefore, no additional tie-breaking rule was required. The classified maps derived from the trained SVM configurations were finally validated against the ground-truth dataset, allowing an accurate reconstruction of the current spatial distribution of *Ailanthus altissima* within the reserve and the identification of the model configuration providing the best classification performance.

The integration of UAV-derived reference data with satellite-based classification represents a key methodological strength of this experiment, as it establishes a multi-scale validation framework that links fine-scale ground information with coarser-resolution remote sensing data, thereby improving the robustness and reliability of the overall classification approach.

2.5. Assessment of the optimal SVM configuration

To investigate classification performance under varying levels of model complexity, the six kernel configurations presented in Section 2.4 (i.e., Linear, Quadratic, Cubic, and Gaussian kernels with Fine, Medium, and Coarse) were evaluated. This allowed a direct comparison of the relative flexibility and non-linear capacity of each SVM type.

The actual evaluation and selection of the optimal SVM configuration were performed on the independent study site "*Vallone Piano della Corte*", ensuring unbiased assessment. Application of the trained models to this site produced six classified maps (one per kernel configuration), which were compared against the independent validation map derived from UAV and field surveys (Fig. 5).

The comparative assessment of different SVM kernels was conducted within a controlled experimental setting, where all models were trained under identical conditions, allowing for a consistent and unbiased benchmarking of their respective performances.

Performance was assessed through confusion matrices allowing the determination of true positives (TP; correct classifications, diagonal elements), false positives and false negatives (FP and FN, respectively; misclassifications, off-diagonal elements). From these, both class-specific indicators and global accuracy measures were derived (Chicco et al., 2021; Maxwell et al., 2021). Precision (i.e., user's accuracy) and recall (i.e., producer's accuracy) were calculated for each class. Precision, defined as in Eq. 1

$$Precision = \frac{TP}{TP + FP} 100\ [\%] \tag{Eq. 1}$$

measures the proportion of pixels assigned to a given class that are correct, thus reflecting the reliability of model predictions. Recall, expressed in Eq. 2

$$Recall = \frac{TP}{TP + FN} 100\ [\%] \tag{Eq. 2}$$

quantifies the proportion of true reference pixels of a class that are correctly identified, providing an indication of the model's ability to capture all occurrences of that class. Both precision and recall indexes range from 0 to 100%, with values closer to 100% indicating better classification performance. If only one of these metrics is high, it reflects a trade-off: high precision with low recall indicates that the model is conservative, while high recall with low precision indicates that it captures most occurrences but includes more misclassifications.

Given the strong class imbalance characterizing the AOI, with *Ailanthus altissima* representing a rare class occupying a limited spatial extent compared to the other land cover classes, which dominate the landscape, particular care was taken in interpreting pixel-based accuracy metrics. Under such conditions, low class prevalence may lead to apparently poor performance indicators even when the target class is effectively detected in space, a phenomenon commonly referred to as the prevalence paradox (Chen et al., 2025). For this reason, the F1 score was also computed, a particularly informative metric under strong class imbalance (Eq. (3)):

$$F1 = 2\frac{Precision^{*}Recall}{Precision + Recall} \tag{Eq. 3}$$

The overall classification performance was first evaluated using the Overall Accuracy (*OA*), which measures the proportion of correctly classified samples over the total (Eq. (4)):

$$OA = \frac{(TP + TN)}{TP + TN + FP + FN} \tag{Eq. 4}$$

To account for agreement beyond chance, Cohen's Kappa (k) was also computed (Eq. (5)):

$$k = \frac{p_o - p_e}{1 - p_e} \tag{Eq. 5}$$

where p_o is the observed agreement (i.e., the *OA*) and p_e the expected agreement by chance.

It is worth noting that global accuracy measures such as *OA* and k may also be influenced by class prevalence and imbalance, thus motivating the use of Balanced Accuracy (*BA*) as an additional global metric (Eq. (6)).

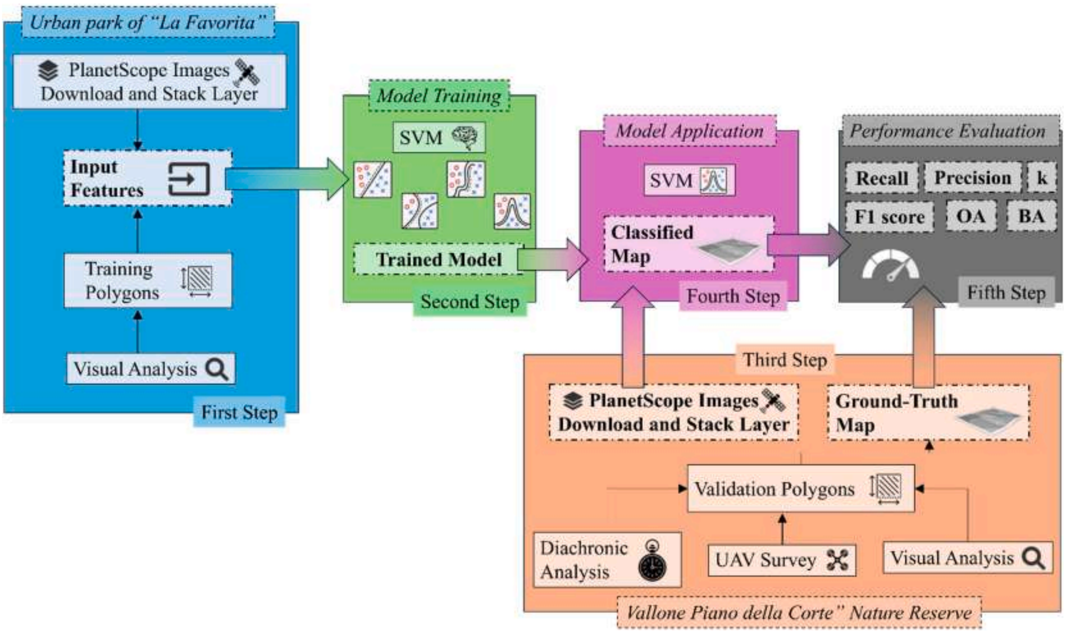

Fig. 6. Flowchart summarizing the five main steps of the proposed methodology. Colored background rectangles are used to distinguish each step. Each step is identified by a dashed box containing its label in italic text. Within each step, intermediate procedures are represented by boxes sharing the same color as the main step but in a lighter shade and with a solid outline. The outputs of each step are shown in boxes with a dash–dot border and bold text.

$$BA = \frac{1}{C}\sum_{i=1}^{C}\frac{TP_i}{TP_i + FN_i} \tag{Eq. 6}$$

where C is the number of classes, and TP_i and FN_i refer to true positives and false negatives for class i, respectively.

The following sections present results in detail, first focusing on per-class performance and error patterns, and synthesizing them into global measures of agreement across the different SVM configurations. It is worth noting that none of the SVM configurations identified any pixels belonging to the urban or water classes within the study area, consistent with their actual absence; therefore these two classes are not discussed further in the next sections.

Fig. 6 provides a reproducibility-oriented overview of the complete workflow, summarizing the main processing steps from raw PlanetScope imagery acquisition and preprocessing, through multitemporal feature construction, SVM training, model application, and independent validation using UAV-derived reference data.

3. Results

3.1. Class-specific performance and error analysis

Confusion matrices (Fig. 7) for the six SVM configurations reveal substantial variability in the classification of individual land cover types. Values on the diagonal represent correctly classified pixels (TP) for each class, while off-diagonal values correspond to misclassified pixels (FP and FN). Row sums indicate the total number of pixels belonging to each class in the validation map, and column sums show the total number of pixels assigned to each class in the classified maps.

Detecting *Ailanthus altissima* is consistently difficult, mainly due to its limited presence in the study area and its spectral similarity to surrounding vegetation. More specifically, for *Ailanthus altissima*, which in the reference validation map accounted for 331 pixels, the Linear SVM (Fig. 7 (a)) correctly identified 58 TP, while producing 21 FP and missing 273 true occurrences (FN). The Quadratic kernel (Fig. 7 (b)) achieved 24 TP, with no FP, but 307 FN, whereas the Cubic kernel (Fig. 7 (c)) slightly improved detection with 38 TP, 4 FP, and 293 FN. The Fine Gaussian kernel (Fig. 7 (d)) reached 30 TP, 1 FP, and 301 FN. The Medium Gaussian kernel (Fig. 7 (e)) performed very poorly: it detected only 3 true pixels, did not misclassify any others, but failed to recognize 328 actual occurrences, highlighting an extreme case where the classification model is overly conservative. Finally, through the Coarse Gaussian kernel (Fig. 7 (f)) the

(a)

[px] Observed classes / Predicted classes	Ailanthus	Bare soil	Other vegetation	Σ
Ailanthus	58	6	267	331
Bare soil	9	5947	1648	7604
Other vegetation	12	670	11624	12306
Σ	79	6623	13539	20241

(b)

[px] Observed classes / Predicted classes	Ailanthus	Bare soil	Other vegetation	Σ
Ailanthus	24	90	217	331
Bare soil	0	7555	49	7604
Other vegetation	0	2168	10138	12306
Σ	24	9813	10404	20241

(c)

[px] Observed classes / Predicted classes	Ailanthus	Bare soil	Other vegetation	Σ
Ailanthus	38	95	198	331
Bare soil	0	7533	71	7604
Other vegetation	4	2225	10077	12306
Σ	42	9853	10346	20241

(d)

[px] Observed classes / Predicted classes	Ailanthus	Bare soil	Other vegetation	Σ
Ailanthus	30	6	295	331
Bare soil	1	5989	1614	7604
Other vegetation	0	682	11624	12306
Σ	31	6677	13533	20241

(e)

[px] Observed classes / Predicted classes	Ailanthus	Bare soil	Other vegetation	Σ
Ailanthus	3	162	166	331
Bare soil	0	7588	16	7604
Other vegetation	0	3209	9097	12306
Σ	3	10959	9279	20241

(f)

[px] Observed classes / Predicted classes	Ailanthus	Bare soil	Other vegetation	Σ
Ailanthus	214	99	18	331
Bare soil	15	7566	23	7604
Other vegetation	227	2531	9548	12306
Σ	456	10196	9589	20241

Fig. 7. Confusion matrices for all SVM configurations (Linear (a), Quadratic (b), Cubic (c), Fine Gaussian (d), Medium Gaussian (e), and Coarse Gaussian (f)), obtained by comparing the classified maps of the AOI with the reference validation map in the same area.

model correctly identified 214 pixels of *Ailanthus*, but also 242 FP and 117 FN were observed.

For the abundant classes, classification performance was consistently higher. Bare soil, which comprised 7604 pixels in the reference map, showed true positives ranging from 5947 (Linear SVM) to 7588 (Medium Gaussian), with false positives between 676 (Linear) and 3371 (Medium Gaussian), and false negatives between 16 (Medium Gaussian) and 1657 (Linear). Other vegetation, representing 12306 pixels in the reference dataset, achieved true positives between 9097 (Medium Gaussian) and 11624 (Linear and Fine Gaussian), with FP ranging from 41 (Coarse Gaussian) to 1915 (Linear), and FN from 682 (Linear and Fine Gaussian) to 3209 (Medium Gaussian). As shown in Fig. 7(a–f), analysis of misclassifications for *Ailanthus altissima* further highlights the differences between kernels. The Medium Gaussian kernel produced the highest error: out of 331 pixels, 162 (∼49%) were misclassified as bare soil and 166 (∼50%) as other vegetation, meaning almost all pixels were incorrectly assigned. The Coarse Gaussian kernel showed the lowest misclassification rate, with only 99 pixels (∼30%) labeled as bare soil and 18 pixels (∼5%) as other vegetation. For all the kernels, the main source of error was misclassification as other vegetation, while confusion with bare soil remained relatively limited.

Overall, these results highlight the inherent trade-off between detecting the minority *Ailanthus* class and preserving high accuracy for the dominant land cover types. All SVM configurations performed robustly on bare soil and other vegetation; however, only the Coarse Gaussian kernel achieved a meaningful detection of *Ailanthus*, correctly identifying more than half of its occurrences. These improvements, though, came at the expense of a substantial increase in false positives, underscoring the difficulty of reliably mapping *Ailanthus* without compromising performance on the majority classes.

To better interpret these outcomes, precision (i.e., user's accuracy) and recall (i.e., producer's accuracy) were calculated for each class (Fig. 8).

For the *Ailanthus altissima* class, the results reported in Fig. 8 reveal markedly different behaviors depending on the kernel configuration used. Polynomial models (Quadratic and Cubic) and the Fine Gaussian kernel were extremely conservative: in these cases, precision was very high (up to 100%), but recall remained very low, below 12%. In other words, these configurations classified pixels as *Ailanthus* only in "safe" situations, avoiding almost all false positives, but systematically missing the majority of true occurrences. The Linear SVM achieved intermediate performance, with a precision of 73% and a recall of 18%, providing a slightly more balanced, yet still largely ineffective, detection. The apparently perfect precision of the Medium Gaussian kernel is misleading: only 3 pixels were identified as *Ailanthus*, all of which were correctly classified, giving a precision of 100%. This configuration fails to detect the *Ailanthus* pixels, as reflected by its extremely low recall of just 9%, indicating that almost all true occurrences were missing. In contrast, the Coarse Gaussian kernel clearly outperformed the others in terms of recall (65%), capturing most of the *Ailanthus* occurrences, though at the expense of lower precision (47%) due to a substantial number of false positives.

For the bare soil class, precision values ranged from 69% (Medium Gaussian) to 90% (Linear), reflecting how often pixels classified as bare soil were correct. Recall spanned from 78% (Linear) to almost 100% (Medium and Coarse Gaussian), indicating the proportion of true bare soil pixels correctly detected. This highlights a clear trade-off: kernels like Linear and Fine Gaussian achieve high precision (90%) but lower recall (78% and 79%, respectively) missing a significant number of true bare soil pixels. Conversely, Quadratic, Medium Gaussian, and Coarse Gaussian achieve very high recall (99% – 100%), capturing nearly all true bare soil pixels, but at the cost of lower precision (69% – 77%) due to misclassification of non-bare soil pixels.

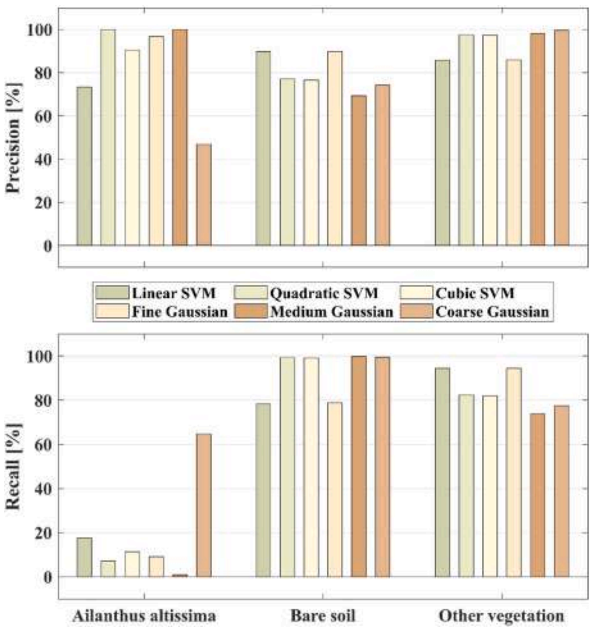

Fig. 8. Class-specific precision (top panel) and recall (bottom panel) for the six SVM configurations. Bars are grouped by land cover class (*Ailanthus altissima*, bare soil, and other vegetation), with colors representing the different SVM kernels.

Finally, for the other vegetation class, precision ranged from 86% (Linear and Fine Gaussian) to almost 100% (Coarse Gaussian), indicating that most pixels predicted as other vegetation were correct. Recall varied from 74% (Medium Gaussian) to 94% (Linear and Fine Gaussian), reflecting the proportion of true other vegetation pixels correctly detected. Overall, all kernel configurations performed reliably for this abundant class. High precision in Coarse and Medium Gaussian (98% and almost 100%, respectively) ensured few false positives, while recall showed more variability: Linear and Fine Gaussian recovered over 94% of true pixels, whereas Medium and Coarse Gaussian missed a larger fraction (74% and 78%, respectively), indicating that some genuine other vegetation pixels were not captured.

To balance precision and recall under strong class imbalance, F1 score was evaluated as a further accuracy metric (Table 1).

The results reported in Table 1 confirm again that *Ailanthus altissima* is consistently the most difficult class to detect, with F1 values below 0.28 for most kernel configurations. Only the Coarse Gaussian kernel achieved a substantially higher F1 (0.54), reflecting a better balance between omission and commission errors. In contrast, the abundant classes (bare soil and other vegetation) achieved much higher F1 scores (0.87 and 0.90, respectively), confirming their robust classification across all kernel configurations. This pattern is expected, as the classification task involves first separating vegetation from non-vegetation and then identifying a rare occurrence (i.e., *Ailanthus altissima*) within the vegetated areas. Low F1 scores for rare species are therefore common in such hierarchical or imbalanced classification schemes.

In summary, the class-specific error analysis highlights that detecting *Ailanthus altissima* remains the main challenge. The Coarse Gaussian kernel represents a compromise solution, capturing a substantial portion of *Ailanthus altissima* occurrences while maintaining reliable performance for the dominant land cover classes.

3.2. Overall classification accuracy and agreement

The overall classification performance was evaluated using the Overall Accuracy (*OA*) and the Cohen's Kappa (*k*); moreover, an additional metric accounting for class imbalance was considered, i.e., the Balanced Accuracy (*BA*) (Table 2).

The comparison of overall performance metrics highlights clear differences among the SVM kernel configurations. *OA* is consistently high across all models, ranging from 82.4% (Medium Gaussian) to 87.5% (Quadratic), with the Quadratic kernel achieving the highest performance, closely followed by the Cubic, Fine Gaussian, and Linear configurations. Cohen's Kappa follows a similar pattern, with the highest agreement observed for the Quadratic configuration (0.753), followed by Cubic (0.747) and Linear (0.726), whereas the Medium Gaussian configuration again yields the lowest value (0.661). However, *OA* and *k* primarily reflect global agreement and may not fully capture the effect of uneven class distribution. Balanced accuracy (*BA*) provides a complementary perspective by emphasizing the ability of the models to correctly classify both dominant and less represented classes. In this case, the Coarse Gaussian kernel clearly outperforms all other configurations (80.6%), while the remaining models show lower and relatively comparable values, with Cubic (64.1%), Linear (63.4%), and Quadratic (63%) slightly outperforming Fine (60.8%) and Medium Gaussian (58.2%).

These results indicate an improved ability of the Coarse Gaussian configuration to balance class-wise performance, particularly in detecting *Ailanthus altissima* within the AOI. Taken together, these findings show that while the Quadratic (and to a slightly lesser extent, Cubic) kernel achieves the highest overall agreement in terms of OA and k, the Coarse Gaussian configuration provides a more balanced classification performance, representing a valuable option when the detection of less represented classes is of primary importance (Fig. 9).

Fig. 9 shows a strong overall agreement with the validation map, accurately reproducing the main land cover patterns within the "*Vallone Piano della Corte*" AOI. The locations of *Ailanthus altissima* nuclei are generally well captured, while the distribution of the other vegetation class and most of the bare soil areas are consistently identified. Some discrepancies remain for isolated tree elements, which should have been classified as other vegetation but were instead mapped as bare soil, highlighting local limitations in class separability.

Focusing on *Ailanthus altissima*, the species is overall well delineated, with most of the main nuclei correctly mapped. However, one nucleus was not properly detected, and localized misclassifications are present in the form of both false positives and false negatives (Fig. 10).

Fig. 10 shows that most of the main nuclei are correctly detected (TP, green pixels), confirming the Coarse Gaussian configuration's ability to capture the general distribution of the species. However, although the total number of false positives (FP, red pixels) and false negatives (FN, yellow pixels) exceed that of TP at the pixel level, this outcome should be interpreted considering the low prevalence of *Ailanthus altissima* within the AOI. Compared to other, more extensive land cover classes, *Ailanthus altissima* occupies a small fraction of the area. Under such conditions, TP pixels form spatially coherent clusters corresponding to the main *Ailanthus* nuclei, while FP and FN pixels are mainly located along patch boundaries and transitional zones.

A substantial portion of the false negatives occurs within one of the *Ailanthus* clusters dominated by very young individuals with

Table 1
Class-specific F1 scores for the six SVM configurations.

	SVM kernel configurations					
	Linear	Quadratic	Cubic	Fine Gaussian	Medium Gaussian	Coarse Gaussian
Ailanthus altissima	0.28	0.14	0.20	0.17	0.02	0.54
Bare soil	0.84	0.87	0.86	0.84	0.82	0.85
Other vegetation	0.90	0.89	0.89	0.90	0.84	0.87

Table 2
Overall classification performance of the six SVM configurations. Reported metrics include Overall Accuracy (*OA*), Cohen's Kappa (*k*), and Balanced Accuracy (*BA*).

	SVM kernel configurations					
	Linear	Quadratic	Cubic	Fine Gaussian	Medium Gaussian	Coarse Gaussian
OA	87.1%	87.5%	87.2%	87.2%	82.4%	85.6%
k	0.726	0.753	0.747	0.727	0.661	0.724
BA	63.4%	63.0%	64.1%	60.8%	58.2%	80.6%

Fig. 9. Final land cover classification map of the "*Vallone Piano della Corte*" AOI obtained using the Coarse Gaussian SVM.

sparse, poorly developed canopies. Under these conditions, the 3 m pixel footprint includes a significant portion of exposed soil, resulting in radiometric responses that resemble bare soil more closely than mature *Ailanthus* trees. This spectral ambiguity makes early-stage stands particularly difficult to distinguish.

A plausible source of the observed false positives is, instead, the smoothing effect introduced by the cubic convolution resampling applied to the raw PlanetScope imagery before being released to the public. Because each output pixel is interpolated from a 4x4 neighborhood of raw data, sharp transitions between land cover types are softened. This smoothing can broaden the apparent spatial extent of spectrally distinctive targets, causing class boundaries to "bleed" into adjacent areas. As a result, pixels located along the edges of *Ailanthus altissima* patches may acquire mixed or intermediate spectral signatures that increase the likelihood of being assigned to the target class even when only partially covered by the species.

These findings show how both biological factors, like life stage and canopy density of the individual, and sensor-level effects, such as resampling-induced smoothing, jointly affect species detectability. Despite these, the Coarse Gaussian kernel consistently identified the majority of *Ailanthus* nuclei while maintaining high accuracy across dominant land cover classes, confirming it as the most suitable configuration for operational mapping in the study area. This choice is further supported by the results of statistical significance analysis accounting for multiple comparisons among model configurations (see Supplementary Material). The analysis confirms that differences among SVM configurations are statistically significant and become more pronounced when focusing on the *Ailanthus altissima* class. In particular, the Coarse Gaussian configuration shows a statistically stronger performance in detecting the minority class compared to the other configurations, reinforcing its suitability under class-imbalanced conditions.

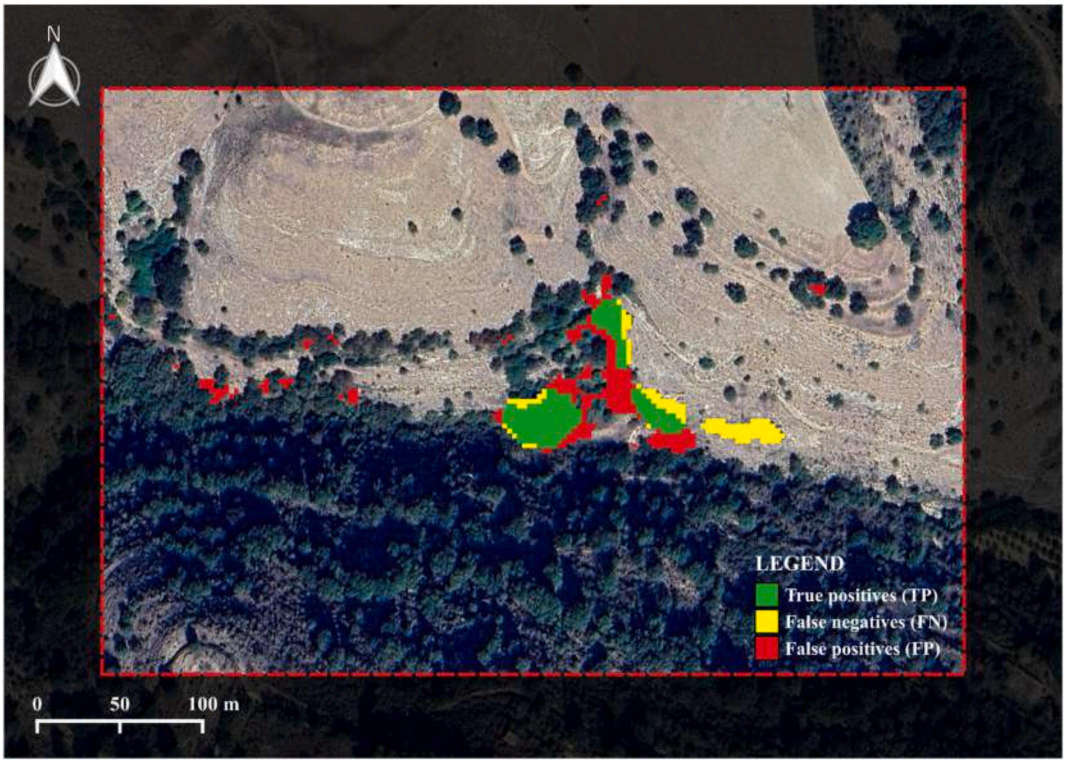

Fig. 10. Comparison between the classification map obtained using Coarse Gaussian SVM kernel and the validation map for the *Ailanthus altissima* class. Green pixels represent true positives (TP), i.e., nuclei correctly identified by the Coarse Gaussian SVM. Yellow pixels indicate false negatives (FN), i.e., true *Ailanthus* occurrences that were missed and assigned to other classes. Red pixels correspond to false positives (FP), areas that were classified as *Ailanthus,* but where the species is absent. The background image is a natural color optical image obtained from Google Earth.

4. Discussion

This study demonstrates the potential of supervised machine learning classification, specifically the Support Vector Machine (SVM) algorithm, for mapping the spatial distribution of *Ailanthus altissima* in Mediterranean environments, while also revealing the inherent limitations of this approach. Across the tested SVM kernel configurations, a clear trade-off between precision and recall emerged. Polynomial (Quadratic and Cubic) and Fine Gaussian kernels proved highly conservative, achieving remarkably high precision but extremely low recall (<12%), and thus systematically missing most occurrences of *Ailanthus altissima*. Linear SVM provided intermediate performance, moderately balancing precision and recall. In contrast, the Coarse Gaussian kernel improved recall (65%), capturing most *Ailanthus* occurrences while maintaining moderate precision (47%). For the more abundant classes (bare soil and other vegetation), all kernel configurations performed consistently well, with misclassifications primarily occurring within these classes and only limited confusion with *Ailanthus altissima*. These results confirm that the primary challenge in the AOI lies in detecting the spatially rare invasive species rather than in discriminating among dominant vegetation types. The pronounced imbalance between *Ailanthus altissima* and surrounding land-cover classes reflects the ecological structure of the AOI, where the invasive species occupies a small portion of the landscape compared to extensive areas of bare soil and native or semi-natural vegetation.

Although global accuracy metrics such as Overall Accuracy and Cohen's Kappa were high across all kernel configurations, these metrics alone provide an incomplete representation of model performance under conditions of strong class imbalance. This aspect represents a key distinction of the present work, which explicitly focuses on how different model configurations behave under class imbalance conditions, rather than relying solely on global accuracy measures. Furthermore, the strong imbalance between *Ailanthus altissima* and the dominant land-cover classes introduces greater uncertainty in minority-class performance estimates, requiring careful interpretation of class-specific metrics despite the use of imbalance-aware evaluation measures such as F1-score and Balanced Accuracy. Balanced Accuracy (*BA*), which accounts for the prevalence paradox, proved more informative for evaluating model performance. Using this metric, the Coarse Gaussian kernel was confirmed as the most effective compromise between detecting *Ailanthus altissima* and reliably classifying dominant classes with a *BA* equal to 80.6%. Although the statistical significance analyses confirmed meaningful differences among the tested SVM configurations, model selection was not based exclusively on statistical significance. Greater importance was assigned to the practical relevance of the results, namely the ability to reliably detect *Ailanthus altissima* under strong class-imbalance conditions and to support operational monitoring activities. In this context, the superior performance of the Coarse Gaussian kernel is particularly meaningful because it translates into a substantially improved detection of invasion nuclei, which is the primary objective of the proposed framework. These findings underscore the importance of selecting evaluation metrics that are appropriate for rare-species detection and highlight how kernel choice can influence the ecological interpretability of machine learning outputs in invasive species mapping.

The results observed in this study align with a growing body of literature highlighting both the potential and the limitations of remote sensing-based approach for invasive alien species detection, particularly when the target species is spatially rare and embedded within heterogeneous landscapes. High overall classification accuracies, often exceeding 80–90%, are commonly reported in remote sensing studies of invasive species detection (Tarantino et al., 2019; Rebelo et al., 2021). However, such global metrics can mask substantial differences in detectability for minority classes. Rebelo et al. (2021) highlighted that, although alien vegetation can generally be discriminated from dominant land-cover types, herbaceous or sparsely distributed invasive species remain difficult to detect even when using high-resolution or hyperspectral data. Similarly, Sentinel-2-based studies coupled with SVM classifiers have achieved overall accuracies in the 80–90% range for invasive woody vegetation mapping, with SVM often outperforming alternative methods such as Random Forest. Nevertheless, these approaches consistently report reduced performance for spatially rare or spectrally heterogeneous species occurring at low abundance within complex landscapes.

Tarantino et al. (2019) similarly noted that comparisons among studies are hindered by differences in temporal sampling, input data, as well as a lack of species-level error analysis. By explicitly analyzing class-specific precision and recall, as well as the behavior of different SVM configurations under class imbalance, this study addresses these gaps and demonstrates that high global accuracy can mask poor detection of rare species under strong class imbalance.

In contrast to many previous studies that primarily report overall accuracy metrics or focus on model comparison at the algorithm level (Qian et al., 2020; Rebelo et al., 2021), the present work explicitly investigates how classifier behavior changes under strong class imbalance conditions, with a specific focus on class-level detectability of a rare invasive species.

Methodologically, this study also complements and extends prior work. While UAV studies (Naharki et al., 2023) achieve near-complete detection under highly controlled conditions (low-altitude flights, specific phenological stages, and multiple optical or thermal sensors), detection at landscape scale using satellite imagery is inherently limited by spectral mixing, spatial fragmentation, and background complexity. Unlike previous efforts that focused primarily on optimizing data acquisition (multitemporal imagery, UAV flights, or sensor fusion), the presented approach isolates classification model-driven effects, systematically evaluating how SVM kernel configuration alone influences detection performance for a spatially rare invasive species. This highlights that mapping behavior can emerge purely from algorithm choice, even when global accuracy remains high, and demonstrates direct ecological implications for operational monitoring. Moreover, recent UAV-based deep learning approaches have reported very high classification performances for invasive plant detection, with accuracies exceeding 90% (Qian et al., 2020), benefiting from ultra-high spatial resolution and controlled acquisition conditions. However, such approaches operate at very fine spatial scales and are not directly transferable to landscape-scale monitoring using satellite images.

Across these studies, a common theme emerges: limitations in invasive species mapping are often ecological and structural rather than purely technical. Low prevalence, spatial fragmentation, and phenological variability impose inherent constraints on detectability across sensors and platforms. The present study advances the literature by explicitly framing classification model performance through the lens of the prevalence paradox and by demonstrating how kernel-dependent behavior in SVM algorithm can lead to substantially different outcomes under class imbalance conditions, even when overall accuracy remains high. A further consideration concerns the transferability assessment of the proposed framework. Although the use of spatially independent training and validation areas provides a more rigorous evaluation than conventional within-site validation approaches, the assessment was conducted using a single independent validation site. Therefore, while the results are encouraging, additional applications across study areas characterized by different environmental conditions, landscape compositions, and invasion patterns would be beneficial to further evaluate the generalizability and robustness of the proposed framework.

5. Conclusions

This study demonstrates that supervised machine learning classification, applied to multitemporal satellite images, provides an effective and operational framework for mapping *Ailanthus altissima* in Mediterranean landscapes. The explicit integration of ecological knowledge of species phenology, spatial structure, and invasion dynamics with multitemporal satellite images and machine learning classification proved essential for distinguishing the species from surrounding vegetation. This study demonstrates how remote sensing can be transformed from a purely technical mapping tool into an ecologically informed framework for invasive species monitoring and management. Within this broader framework, the main conclusions emerging from the work can be articulated around a series of interconnected aspects:

- Operational performance of the classification model: among the tested configurations, the Coarse Gaussian kernel provided the most balanced compromise between detecting *Ailanthus* occurrences and maintaining reliable classification of the dominant land cover types (i.e., bare soil and other vegetation). While this configuration achieved better outcomes than the other kernels, detection performance remained constrained by the rarity and heterogeneous structure of the target species. The observed performance can be attributed to the kernel's ability to model complex, non-linear relationships in the high-dimensional spectral-temporal feature space but also highlights the inherent trade-off between sensitivity and specificity when mapping a spatially rare invasive species. Detection accuracy was strongly influenced by life stage, canopy density, and spatial arrangement of the species, with sparse or juvenile individuals often remaining below detectability, and some false positives arising from spectral similarity to neighboring vegetation or lightly vegetated soil. These limitations are further influenced by the spatial resolution of PlanetScope imagery, which can restrict the detection of small or juvenile individuals whose canopy extent may remain below the 3 m pixel size even during peak growing conditions. This constraint contributes to mixed-pixel effects at class boundaries and may reduce detection sensitivity for early-stage invasion patterns.

The effectiveness of the Coarse Gaussian configuration is expected to extend to other datasets with spatial resolutions comparable to PlanetScope resolution, where *Ailanthus* nuclei occupy multiple pixels, allowing the kernel to exploit spatial and spectral coherence. Higher spatial resolution datasets could potentially improve the detection of smaller individuals; however, maintaining equivalent multitemporal coverage would require a substantially larger volume of data and a higher computational burden, which are often associated with higher acquisition costs. In this context, the present approach demonstrates how multitemporal satellite data with moderate spatial resolution can still provide effective and operationally viable detection of *Ailanthus altissima* in ecologically sensitive areas such as natural reserves and parks. Despite these potential variations, the underlying principle that a sufficiently flexible non-linear SVM kernel can effectively capture species-specific spectral-temporal signatures is broadly applicable to multitemporal classification of rare or challenging target species, making this approach conceptually transferable beyond the specific PlanetScope dataset.

- Role of multitemporal imagery: the use of multi-year PlanetScope data was essential, as phenological dynamics provided the separability needed to distinguish *Ailanthus* from co-occurring species. By incorporating both seasonal and interannual changes, the classification model could capture patterns that are not evident in single-date imagery, improving detection of mature *Ailanthus* nuclei. However, the sensor's moderate spatial resolution introduces limitations in detecting small, isolated patches or early-stage individuals, whose sparse canopies produce mixed spectral signals with surrounding soil or vegetation. Despite this, the temporal dimension remains a critical factor in enhancing model performance and robustness for monitoring this invasive species.
- Potential of cross-site training and model transferability: a notable strength of the work lies in the use of a training site ("*La Favorita*" Urban Park) distinct from the application site ("*Vallone Piano della Corte*" Nature Reserve). Despite spatial separation, both areas share relevant ecological and structural characteristics, including mosaics of woody vegetation, exposed or sparsely vegetated soils, and established *Ailanthus* nuclei. Under these conditions, the approach demonstrated two key advantages: first, the classification model showed the ability to generalize beyond the site where it was calibrated, successfully reproducing the spatial distribution of *Ailanthus altissima* in an independent area; second, this experimental design provided a more rigorous and realistic evaluation of model transferability compared to conventional approaches based on within-site validation.
- Implication for ecological monitoring and management: the results indicate that the proposed approach is particularly promising when used in combination with complementary drone-based and ground surveys at local scales, rather than as a stand-alone mapping solution. While the satellite-based classification is effective in identifying the general location of *Ailanthus altissima* nuclei, fine-scale delineation and confirmation of invaded patches benefit substantially from targeted UAV observations and field inspections. In this context, the approach enables a shift from exhaustive field mapping to targeted validation, allowing field surveys to be concentrated on priority areas identified through satellite-based detection, thereby substantially reducing time, costs, and logistical effort. More importantly, the proposed approach, combining multitemporal satellite imagery with flexible SVM classification, shows promising potential for application at broader regional scales, enabling the identification of emerging invasion hotspots, assessment of the expansion of occupied areas, and early-warning monitoring for proactive management. However, additional validation across study areas characterized by different environmental conditions, landscape structures, and invasion patterns would be beneficial to further assess the transferability and robustness of the proposed framework. The satellite-based framework offers operational scalability, allowing consistent, repeatable, and cost-effective mapping across large landscapes. From a management perspective, the main ecological value of the derived maps lies in supporting decision-making by guiding field activities towards areas with a higher likelihood of invasion, optimizing resource allocation, and enabling timely intervention before nuclei expand. This targeted strategy is particularly advantageous in protected or hard-to-access environments, where comprehensive field surveys would otherwise be time-consuming and resource-intensive. In addition, the derived maps can be used not only as stand-alone products, but also as inputs for ecohydrological or vegetation-dynamics models, enabling scenario-based simulations under different environmental and climatic conditions.
- Scalability, replicability, and decision-support potential: the reliance on multitemporal satellite images with consistent spatial, spectral, and temporal characteristics makes the proposed workflow potentially scalable and replicable across space and time. Once trained, the classification framework could be applied to larger geographic extents without the need for extensive site-specific field campaigns, supporting regional-scale screening and repeated monitoring. This scalability, combined with the observed cross-site transferability, suggests potential for early-stage invasion detection and prioritization of management interventions. Rather than replacing detailed field surveys, the approach provides a decision-support tool to guide targeted inspections, optimize resource allocation, and support proactive management strategies aimed at preventing further spread of *Ailanthus altissima.*

In conclusion, this work establishes a practical and adaptable workflow for mapping invasive species that combines a machine learning algorithm, multitemporal remote sensing images, and ecological knowledge. The proposed approach proves effective in correctly identifying the spatial location of *Ailanthus altissima* nuclei, enabling reliable detection and localization of invaded areas; however, it shows limited precision in delineating their exact spatial extent, resulting in accurate localization without a complete characterization of patch boundaries. The results indicate that the proposed framework should be interpreted as an exploratory and preliminary approach, aimed at evaluating the feasibility, strengths, and limitations of satellite-based machine learning for detecting a spatially rare invasive species under realistic operational conditions. Within this scope, the approach proves effective for current monitoring needs while clearly revealing the constraints imposed by class imbalance, satellite products resampling method, and ecological heterogeneity of the invasive species, even without the knowledge of their phenological and structural characteristics. Thus, the detection performance could potentially be enhanced by explicitly incorporating specific traits, such as canopy architecture (e.g., canopy size), and growth stage (e.g., diameter at breast height, tree height). While effective for current operational needs, the identified limitations point to promising directions for future studies. These include the integration of finer spatial resolution sensors (drone, WorldView 2/3, Pleiades, etc.) and hyperspectral imagery to improve detection of small, juvenile, or sparsely canopied individuals, the use of raw radiometric data to avoid smoothing artifacts introduced by cubic-convolution resampling, and the application of data fusion approaches to combine complementary information from multiple sensors. Additional opportunities involve increasing the temporal frequency of acquisitions, incorporating structural data such as LiDAR or canopy height metrics, and exploring advanced machine learning methods, including deep learning, to better capture complex spectral-spatial patterns.

CRediT authorship contribution statement

Francesco Alongi: Conceptualization, Data curation, Formal analysis, Investigation, Methodology, Software, Validation, Visualization, Writing – original draft, Writing – review & editing. **Dario De Caro:** Conceptualization, Data curation, Formal analysis, Investigation, Methodology, Software, Validation, Visualization, Writing – original draft, Writing – review & editing. **Emilio Badalamenti:** Conceptualization, Data curation, Formal analysis, Investigation, Methodology, Software, Validation, Visualization, Writing – original draft, Writing – review & editing. **Fulvio Capodici:** Conceptualization, Methodology, Validation, Visualization, Writing – review & editing. **Rafael Da Silveira Bueno:** Conceptualization, Methodology, Validation, Visualization, Writing – review & editing. **Tommaso La Mantia:** Conceptualization, Funding acquisition, Methodology, Project administration, Supervision, Validation, Visualization, Writing – review & editing. **Giuseppe Ciraolo:** Conceptualization, Funding acquisition, Methodology, Project administration, Supervision, Validation, Visualization, Writing – review & editing. **Leonardo V. Noto:** Conceptualization, Funding acquisition, Methodology, Project administration, Supervision, Validation, Visualization, Writing – review & editing.

Declaration of competing interest

The authors declare that they have no known competing financial interests or personal relationships that could have appeared to influence the work reported in this paper.

Acknowledgments

Project funded under the National Recovery and Resilience Plan (NRRP), Mission 4 Component 2 Investment 1.4 - Call for tender No. 3138 of 16 December 2021, rectified by Decree n.3175 of 18 December 2021 of Italian Ministry of University and Research funded by the European Union – NextGenerationEU Project code CN00000033, Concession Decree No. 1034 of 17 June 2022 adopted by the Italian Ministry of University and Research, CUPB73C22000790001, Project title “National Biodiversity Future Center - NBFC”. Thanks are due to Renzo Ientile, former Director of the “Vallone Piano della Corte” Nature Reserve, managed by the University of Catania, for logistical support during field surveys. We sincerely thank the Reviewers for their thorough and constructive revisions of the manuscript. Their comments and suggestions have significantly improved the clarity, structure, and overall quality of the paper.

Appendix A. Supplementary data

Supplementary data to this article can be found online at https://doi.org/10.1016/j.rsase.2026.102165.

Data availability

Data will be made available on request.

References

Aleo, M., Bazan, G., 2025. Plant diversity and sustainable landscape management: the case of Misiliscemi, a new municipality in sicily. Plants 14, 548. https://doi.org/10.3390/plants14040548.

Anger, J., de Franchis, C., Facciolo, G., 2019. Assessing the sharpness of satellite images. Study of the Planetscope Constellation. https://doi.org/10.48550/ARXIV.1904.09159.

Arnone, E., Pumo, D., Viola, F., Noto, L.V., La Loggia, G., 2013. Rainfall statistics changes in Sicily. Hydrol. Earth Syst. Sci. 17, 2449–2458. https://doi.org/10.5194/hess-17-2449-2013.

Arrington, A., 2021. Urban foraging of five non-native plants in NYC: balancing ecosystem services and invasive species management. Urban For. Urban Green. 58, 126896. https://doi.org/10.1016/j.ufug.2020.126896.

Badalamenti, E., Barone, E., La Mantia, T., 2015a. Seasonal effects on mortality rates and resprouting of stems treated with glyphosate in the invasive tree of heaven (*Ailanthus altissima* (Mill.) Swingle). Arboric. J. 37, 180–195. https://doi.org/10.1080/03071375.2015.1112163.

Badalamenti, E., Barone, E., Pasta, S., Sala, G., La Mantia, T., 2012. Ailanthus altissima (Mill.) Swingle (Simaroubaceae) in Sicilia e cenni storici sulla sua introduzione in Italia. Naturalista siciliano 117–164.

Badalamenti, E., La Mantia, T., Quatrini, P., 2015b. Arbuscular mycorrhizal fungi positively affect growth of *Ailanthus altissima* (Mill.) Swingle seedlings and show a strong association with this invasive species in Mediterranean woodlands. J. Torrey Bot. Soc. 142, 127–139. https://doi.org/10.3159/TORREY-D-14-00034.1.

Badalamenti, E., Sferlazza, S., La Mela Veca, D., Maetzke, F., Sala, G., La Mantia, T., 2020. Which are Southern Italy's fastest growing tree species? Lessons from the past for future perspectives, with a special focus on Sicily. Annals of Silvicultural Research 45. https://doi.org/10.12899/asr-1845.

Badalamenti, E., La Mantia, T., 2013. Stem-injection of herbicide for control of Ailanthus altissima (Mill.) Swingle: a practical source of power for drilling holes in stems. iForest 6, 123–126. https://doi.org/10.3832/ifor0693-006.

Baker, C.M., Blonda, P., Casella, F., Diele, F., Marangi, C., Martiradonna, A., Montomoli, F., Pepper, N., Tamborrino, C., Tarantino, C., 2023. Using remote sensing data within an optimal spatiotemporal model for invasive plant management: the case of Ailanthus altissima in the Alta Murgia National Park. Sci. Rep. 13, 14587. https://doi.org/10.1038/s41598-023-41607-2.

Basheer, S., Wang, X., Nawaz, R.A., Pang, T., Adekanmbi, T., Mahmood, M.Q., 2024. A comparative analysis of PlanetScope 4-band and 8-band imageries for land use land cover classification. Geomatica (Ott.) 76, 100023. https://doi.org/10.1016/j.geomat.2024.100023.

Burges, C.J.C., 1998. A tutorial on support vector machines for pattern recognition. Data Min. Knowl. Discov. 2, 121–167. https://doi.org/10.1023/A:1009715923555.

Campagnaro, T., Brundu, G., Burrascano, S., Celesti-Grapow, L., La Mantia, T., Sitzia, T., Badalamenti, E., 2022. Tree invasions in Italian forests. For. Ecol. Manag. 521, 120382. https://doi.org/10.1016/j.foreco.2022.120382.

Caracciolo, D., Istanbulluoglu, E., Noto, L.V., 2017. An ecohydrological cellular automata model investigation of juniper Tree encroachment in a Western north American landscape. Ecosystems 20, 1104–1123. https://doi.org/10.1007/s10021-016-0096-6.

Caracciolo, D., Istanbulluoglu, E., Noto, L.V., Collins, S.L., 2016. Mechanisms of shrub encroachment into Northern Chihuahuan Desert grasslands and impacts of climate change investigated using a cellular automata model. Adv. Water Resour. 91, 46–62. https://doi.org/10.1016/j.advwatres.2016.03.002.

Caracciolo, D., Noto, L.V., Istanbulluoglu, E., Fatichi, S., Zhou, X., 2014. Climate change and Ecotone boundaries: insights from a cellular automata ecohydrology model in a Mediterranean catchment with topography controlled vegetation patterns. Adv. Water Resour. 73, 159–175. https://doi.org/10.1016/j.advwatres.2014.08.001.

Casella, F., Vurro, M., 2013. *Ailanthus altissima*(tree of heaven): spread and harmfulness in a case-study urban area. Arboric. J. 35, 172–181. https://doi.org/10.1080/03071375.2013.852352.

Celesti-Grapow, L., Ricotta, C., 2021. Plant invasion as an emerging challenge for the conservation of heritage sites: the spread of ornamental trees on ancient monuments in Rome, Italy. Biol. Invasions 23, 1191–1206. https://doi.org/10.1007/s10530-020-02429-9.

Chen, P., Ren, Y., Zhang, B., Zhao, Y., 2025. Class imbalance in the automatic interpretation of remote sensing images: a review. IEEE J. Sel. Top. Appl. Earth Obs. Remote Sens. 18, 9483–9508. https://doi.org/10.1109/JSTARS.2025.3555567.

Chicco, D., Warrens, M.J., Jurman, G., 2021. The Matthews Correlation Coefficient (MCC) is more informative than Cohen's Kappa and brier Score in binary classification assessment. IEEE Access 9, 78368–78381. https://doi.org/10.1109/ACCESS.2021.3084050.

Clements, D.R., 2022. Global Plant Invasions. Springer International Publishing AG, Cham.

Clewley, G.D., Eschen, R., Shaw, R.H., Wright, D.J., 2012. The effectiveness of classical biological control of invasive plants. J. Appl. Ecol. 49, 1287–1295. https://doi.org/10.1111/j.1365-2664.2012.02209.x.

Colberg, E.M., Bradley, B.A., Morelli, T.L., Brown-Lima, C.J., 2024. Climate-Smart invasive species management for 21st century global change challenges. Glob. Change Biol. 30, e17531. https://doi.org/10.1111/gcb.17531.

Constán-Nava, S., Bonet, A., Pastor, E., Lledó, M.J., 2010. Long-term control of the invasive tree Ailanthus altissima: insights from Mediterranean protected forests. For. Ecol. Manag. 260, 1058–1064. https://doi.org/10.1016/j.foreco.2010.06.030.

Cortes, C., Vapnik, V., 1995. Support-vector networks. Mach. Learn. 20, 273–297. https://doi.org/10.1007/BF00994018.

Costa, D., Sutter, C., Shepherd, A., Jarvie, H., Wilson, H., Elliott, J., Liu, J., Macrae, M., 2023. Impact of climate change on catchment nutrient dynamics: insights from around the world. Environ. Rev. 31, 4–25. https://doi.org/10.1139/er-2021-0109.

Culliney, T.W., 2005. Benefits of classical biological control for managing invasive plants. Crit. Rev. Plant Sci. 24, 131–150. https://doi.org/10.1080/07352680590961649.

Demasi, S., Caser, M., Vanara, F., Fogliatto, S., Vidotto, F., Negre, M., Trotta, F., Scariot, V., 2019. Ailanthone from Ailanthus altissima (Mill.) Swingle as potential natural herbicide. Sci. Hortic. 257, 108702. https://doi.org/10.1016/j.scienta.2019.108702.

Ding, J., Wu, Y., Zheng, H., Fu, W., Reardon, R., Liu, M., 2006. Assessing potential biological control of the invasive plant, tree-of-heaven, *Ailanthus altissima*. Biocontrol Sci. Technol. 16, 547–566. https://doi.org/10.1080/09583150500531909.

Frazier, A.E., Hemingway, B.L., 2021. A technical review of planet smallsat data: practical considerations for processing and using PlanetScope imagery. Remote Sens. 13, 3930. https://doi.org/10.3390/rs13193930.

Gao, R., Song, Z., Zhao, J., Li, Y., 2025. Predicting the distribution of Ailanthus altissima using deep learning-based analysis of satellite imagery. Symmetry 17, 324. https://doi.org/10.3390/sym17030324.

Garnier, E., Navas, M.-L., 2012. A trait-based approach to comparative functional plant ecology: concepts, methods and applications for agroecology. A review. Agron. Sustain. Dev. 32, 365–399. https://doi.org/10.1007/s13593-011-0036-y.

Gioria, M., Hulme, P.E., Richardson, D.M., Pyšek, P., 2023. Why are invasive plants successful? Annu. Rev. Plant Biol. 74, 635–670. https://doi.org/10.1146/annurev-arplant-070522-071021.

Giubilei, I., Drais, M.I., Cos, D., Mazzaglia, A., 2025. Occurrence of *Neofusicoccum parvum* associated with dieback of *Ailanthus altissima* in Italy. For. Pathol. 55, e70038. https://doi.org/10.1111/efp.70038.

Graham, N.A.J., Benkwitt, C.E., Jones, H.P., 2024. Species eradication for ecosystem restoration. Curr. Biol. 34, R407–R412. https://doi.org/10.1016/j.cub.2024.02.033.

Guarino, R., Chytrý, M., Attorre, F., Landucci, F., Marcenò, C., 2021. Alien plant invasions in Mediterranean habitats: an assessment for Sicily. Biol. Invasions 23, 3091–3107. https://doi.org/10.1007/s10530-021-02561-0.

Gyamfi-Ampadu, E., Gebreslasie, M., Mendoza-Ponce, A., 2020. Mapping natural forest cover using satellite imagery of Nkandla forest reserve, KwaZulu-Natal, South Africa. Remote Sens. Appl.: Soc. Environ. 18, 100302. https://doi.org/10.1016/j.rsase.2020.100302.

Harvey, E., Gounand, I., Ward, C.L., Altermatt, F., 2017. Bridging ecology and conservation: from ecological networks to ecosystem function. J. Appl. Ecol. 54, 371–379. https://doi.org/10.1111/1365-2664.12769.

Hoffmann, S., 2022. Challenges and opportunities of area-based conservation in reaching biodiversity and sustainability goals. Biodivers. Conserv. 31, 325–352. https://doi.org/10.1007/s10531-021-02340-2.

Kowarik, I., Säumel, I., 2007. Biological flora of central Europe: ailanthus altissima (Mill.) swingle. Perspectives in plant ecology. Evolution and Systematics 8, 207–237. https://doi.org/10.1016/j.ppees.2007.03.002.

Landenberger, R.E., Warner, T.A., McGraw, J.B., 2009. Spatial patterns of female Ailanthus altissima across an urban-to-rural land use gradient. Urban Ecosyst. 12, 437–448. https://doi.org/10.1007/s11252-009-0087-x.

Landi, P., Minoarivelo, H.O., Brännström, Å., Hui, C., Dieckmann, U., 2018. Complexity and stability of ecological networks: a review of the theory. Popul. Ecol. 60, 319–345. https://doi.org/10.1007/s10144-018-0628-3.

Lehan, N.E., Murphy, J.R., Thorburn, L.P., Bradley, B.A., 2013. Accidental introductions are an important source of invasive plants in the continental United States. Am. J. Bot. 100, 1287–1293. https://doi.org/10.3732/ajb.1300061.

Marta, S., 2018. Planet Imagery Product Specifications, 91. Planet Labs, San Francisco, CA, USA, p. 170.

Maxwell, A.E., Warner, T.A., Guillén, L.A., 2021. Accuracy assessment in convolutional neural network-based deep learning remote sensing Studies—Part 1: literature review. Remote Sens. 13, 2450. https://doi.org/10.3390/rs13132450.

Miles, H.H., Salom, S., Shively, T.J., Bielski, J.T., McAvoy, T.J., Fearer, C.J., 2025. A Review of Potential Biological Controls for *Ailanthus altissima*, 118. Annals of the Entomological Society of America, pp. 101–109. https://doi.org/10.1093/aesa/saae041.

Minissale, P., Cambria, S., Montoleone, E., Tavilla, G., Giusso Del Galdo, G., Sciandrello, S., Badalamenti, E., La Mantia, T., 2023. The alien vascular flora of the Pantelleria Island National Park (Sicily Channel, Italy): new insights into the distribution of some potentially invasive species. BIR 12, 861–885. https://doi.org/10.3391/bir.2023.12.4.01.

Motard, E., Dusz, S., Geslin, B., Akpa-Vinceslas, M., Hignard, C., Babiar, O., Clair-Maczulajtys, D., Michel-Salzat, A., 2015. How invasion by Ailanthus altissima transforms soil and litter communities in a temperate forest ecosystem. Biol. Invasions 17, 1817–1832. https://doi.org/10.1007/s10530-014-0838-3.

Motti, R., Zotti, M., Bonanomi, G., Cozzolino, A., Stinca, A., Migliozzi, A., 2021. Climatic and anthropogenic factors affect Ailanthus altissima invasion in a Mediterranean region. Plant Ecol. 222, 1347–1359. https://doi.org/10.1007/s11258-021-01183-9.

Muhammad, M., Wahab, A., Waheed, A., Hakeem, K.R., Mohamed, H.I., Basit, A., Toor, M.D., Liu, Y., Li, L., Li, W., 2025. Navigating climate change: exploring the dynamics between plant–soil microbiomes and their impact on plant growth and productivity. Glob. Change Biol. 31, e70057. https://doi.org/10.1111/gcb.70057.

Naharki, K., Huebner, C.D., Park, Y.-L., 2023. The detection of tree of Heaven (Ailanthus altissima) using drones and optical sensors: implications for the management of invasive plants and insects. Drones 8, 1. https://doi.org/10.3390/drones8010001.

Naora, H., Furuno, T., Ishibashi, M., Tsuyuki, T., Takahashi, T., Itai, A., Iitaka, Y., Polonsky, J., 1982. ON the structure OF ailanthone, a bitter principle from *ailanthus altissima*. Chem. Lett. 11, 661–662. https://doi.org/10.1246/cl.1982.661.

Noto, L.V., Cipolla, G., Francipane, A., Pumo, D., 2023. Climate change in the Mediterranean Basin (Part I): induced alterations on climate forcings and hydrological processes. Water Resour. Manag. 37, 2287–2305. https://doi.org/10.1007/s11269-022-03400-0.

Pisuttu, C., 2024. Verticillium species as an ecofriendly alternative to manage the invasive tree Ailanthus altissima (Mill.) swingle. Forests 15, 462. https://doi.org/10.3390/f15030462.

Planchuelo, G., Catalán, P., Delgado, J.A., Murciano, A., 2017. Estimating wind dispersal potential in *Ailanthus altissima* : the need to consider the three-dimensional structure of samaras. Plant Biosystems - An International Journal Dealing with all Aspects of Plant Biology 151, 316–322. https://doi.org/10.1080/11263504.2016.1174170.

Qian, W., Huang, Y., Liu, Q., Fan, W., Sun, Z., Dong, H., Wan, F., Qiao, X., 2020. UAV and a deep convolutional neural network for monitoring invasive alien plants in the wild. Comput. Electron. Agric. 174, 105519. https://doi.org/10.1016/j.compag.2020.105519.

Rashid, A., Schutte, B.J., Ulery, A., Deyholos, M.K., Sanogo, S., Lehnhoff, E.A., Beck, L., 2023. Heavy metal contamination in agricultural soil: environmental pollutants affecting crop health. Agronomy 13, 1521. https://doi.org/10.3390/agronomy13061521.

Raupp, P., Carrillo, Y., Nielsen, U.N., 2024. Soil health to enhance ecological restoration and conservation. J. Sustain. Agric. Environ. 3, e70022. https://doi.org/10.1002/sae2.70022.

Raven, P., Wackernagel, M., 2020. Maintaining biodiversity will define our long-term success. Plant Divers. 42, 211–220. https://doi.org/10.1016/j.pld.2020.06.002.

Rebbeck, J., Jolliff, J., 2018. How long do seeds of the invasive tree, Ailanthus altissima remain viable? For. Ecol. Manag. 429, 175–179. https://doi.org/10.1016/j.foreco.2018.07.001.

Rebelo, A.J., Gokool, S., Holden, P.B., New, M.G., 2021. Can Sentinel-2 be used to detect invasive alien trees and shrubs in Savanna and Grassland Biomes? Remote Sens. Appl.: Soc. Environ. 23, 100600. https://doi.org/10.1016/j.rsase.2021.100600.

Segar, S.T., Fayle, T.M., Srivastava, D.S., Lewinsohn, T.M., Lewis, O.T., Novotny, V., Kitching, R.L., Maunsell, S.C., 2020. The role of evolution in shaping ecological networks. Trends Ecol. Evol. 35, 454–466. https://doi.org/10.1016/j.tree.2020.01.004.

Shebl, A., Kusky, T., Csámer, Á., 2022. Advanced land imager superiority in lithological classification utilizing machine learning algorithms. Arabian J. Geosci. 15, 923. https://doi.org/10.1007/s12517-022-09948-w.

Shields, S.G., Coops, N.C., Achim, A., Hamelin, R.C., Mulverhill, C., 2025. A review of PlanetScope CubeSats for forest monitoring. Science of Remote Sensing 12, 100314. https://doi.org/10.1016/j.srs.2025.100314.

Sladonja, B., Sušek, M., Guillermic, J., 2015. Review on invasive tree of Heaven (Ailanthus altissima (Mill.) Swingle) conflicting values: assessment of its ecosystem services and potential biological threat. Environ. Manag. 56, 1009–1034. https://doi.org/10.1007/s00267-015-0546-5.

Sladonja, B., Poljuha, D., 2018. Citizen science as a tool in biological Recording—A case Study of Ailanthus altissima (Mill.) swingle. Forests 9, 31. https://doi.org/10.3390/f9010031.

Soler, J., Izquierdo, J., 2024. The invasive ailanthus altissima: a biology, ecology, and control review. Plants 13, 931. https://doi.org/10.3390/plants13070931.

Song, Q., Zhang, W., 2025. Analysis of cultivated land changes and driving factors in the Alar Reclamation Area (1990–2019) based on multi-temporal Landsat data and machine learning algorithms. Sci. Rep. 16, 84. https://doi.org/10.1038/s41598-025-29175-z.

Talmot, V., Hardion, L., Sexton, A., Jumeau, J., Jugieau, E., Staentzel, C., 2025. Environmental conditions affect the allelopathic potential of three invasive alien plants species in North-Eastern France. J. Ecol. 113, 155–167. https://doi.org/10.1111/1365-2745.14447.

Tarantino, C., Casella, F., Adamo, M., Lucas, R., Beierkuhnlein, C., Blonda, P., 2019. Ailanthus altissima mapping from multi-temporal very high resolution satellite images. ISPRS J. Photogrammetry Remote Sens. 147, 90–103. https://doi.org/10.1016/j.isprsjprs.2018.11.013.

Terzi, M., Fontaneto, D., Casella, F., 2021. Effects of Ailanthus altissima invasion and removal on high-biodiversity Mediterranean grasslands. Environ. Manag. 68, 914–927. https://doi.org/10.1007/s00267-021-01522-6.

Treppiedi, D., Villarini, G., Mattina, C., Francipane, A., Noto, L.V., 2026. Unveiling changes in the seasonality of extreme precipitation shows an anticipation of short-duration extremes. Earth Syst. Environ. https://doi.org/10.1007/s41748-026-01178-4.

Trotta, G., Savo, V., Cicinelli, E., Carboni, M., Caneva, G., 2020. Colonization and damages of Ailanthus altissima (Mill.) Swingle on archaeological structures: evidence from the Aurelian Walls in Rome (Italy). Int. Biodeterior. Biodegrad. 153, 105054. https://doi.org/10.1016/j.ibiod.2020.105054.

Trunschke, J., Junker, R.R., Kudo, G., Alexander, J.M., Richman, S.K., Till-Bottraud, I., 2024. Effects of climate change on plant-pollinator interactions and its multitrophic consequences. Alpine Bot. 134, 115–121. https://doi.org/10.1007/s00035-024-00316-w.

Viola, F., Liuzzo, L., Noto, L.V., Lo Conti, F., La Loggia, G., 2014. Spatial distribution of temperature trends in Sicily: spatial DISTRIBUTION of TEMPERATURE trends in sicily. Int. J. Climatol. 34, 1–17. https://doi.org/10.1002/joc.3657.

Wagner, S., Moser, D., Essl, F., 2020. Urban Rivers as dispersal corridors: which factors are important for the spread of alien woody species along the danube? Sustainability 12, 2185. https://doi.org/10.3390/su12062185.

Walker, G.A., Robertson, M.P., Gaertner, M., Gallien, L., Richardson, D.M., 2017. The potential range of Ailanthus altissima (tree of heaven) in South Africa: the roles of climate, land use and disturbance. Biol. Invasions 19, 3675–3690. https://doi.org/10.1007/s10530-017-1597-8.

ZandKarimi, A., Shamsoddini, A., Ebrahimi, O., 2025. Combining multisource remote sensing images using machine learning methods (RF and SVM) for improved cotton field mapping. Remote Sens. Appl.: Soc. Environ. 39, 101645. https://doi.org/10.1016/j.rsase.2025.101645.

Zhang, Yanliang, Zhang, Yuanyuan, Zhang, L., Yang, H., Ma, T., Huang, C., Hu, L., Zhang, M., Sang, W., 2025. Enhanced competitive advantage of invasive plants by growth-defence trade-off: evidence from phytohormone metabolism and transcriptomic analysis. J. Appl. Ecol. 62, 1980–1992. https://doi.org/10.1111/1365-2664.70003.